UNIVERSIDAD DE GUANAJUATO

Centro de Investigaciones en Óptica, A.C.

Study of diode-pumped Nd:YVO_4 lasers passively Q-switched with YAG:Cr^{4+} and LiF:F_2^- crystals.

Thesis submitted in partial fulfillment of the requirements for the degree of:

Doctor in Science (Optics)
Ing. Edgar Villafaña Rauda

Assessor:
Dr. Alexander V. Kir'yanov

November 2004, León, Guanajuato.

Acknowledgments.

Finally, this work has been completed and I would like to thank the following people who made it possible:

A special thanks to Dr. Alexander Kir'yanov who provided me support and expertise.

I would also like to thank to Dr. Victor Pinto for the time I worked with him.

Thanks as well to all my friends for sharing good times.

In addition, I would like to acknowledge the financial support I received from **Consejo Nacional de Ciencia y Tecnología**, México via grant # 129541, **Consejo de Ciencia y Tecnología del estado de Guanajuato** , via grant # 3-04-k119-019 and **Centro de Investigaciones en Óptica, A.C.**

Dedication

This work is dedicated to my wife Maritza whose support and enthusiasm encouraged me to achieve all my dreams.

Contents

Abstract.

In this thesis, CW-pumped Nd:YVO_4 lasers passively Q-switched with LiF:F_2^- and YAG:Cr^{4+} saturable absorbers are modeled and comparatively analyzed. The model takes into account the geometric factor representing the distributions of the orientations of the F_2^- color centers and Cr^{4+} ions relatively to the corresponding crystalline hosts on the output parameters of the lasers. It is shown that the LiF:F_2^- Q-switch has evident advantages over the YAG:Cr^{4+} one, in the senses of a much more expanded range of pump powers where the giant-pulse regime is supported in the laser and, as the consequence, of potentially higher average output and peak pulse powers accessible. Additionally, passive Q-switching (PQS) of a diode-side-pumped Nd:YVO4 laser using a LiF:F2- crystal as a saturable absorber is reported. Applying the grazing-incidence geometry to the cavity, we obtained trains of giant pulses of minimal duration of ~10 ns and peak power of hundreds watts. The laser efficiency and beam quality in the PQS regime are shown to strongly depend on the cavity arrangement and output coupler reflectivity. In particular, maximum of average output of 18.5 W at high-quality (TEM_{00} mode) PQS operation is obtained at pump power of 38 W at the asymmetrical cavity coupled by a mirror with reflectivity 30%. A theoretical modeling of the PQS Nd:YVO4 / LiF:F2- laser is performed as well; its results are demonstrated to be in agreement with the experimental data.

Introduction.

The passive Q-switching (PQS) operation of Neodymium (Nd) lasers based on the ortho-vanadate crystals (Nd:YVO_4, Nd:$GdVO_4$, etc.) is currently under extensive investigation. The Nd-doped ortho-vanadate materials have a big potential in the laser applications because of the larger absorption and emission cross-sections and wider absorption bandwidths compared with the Nd-doped garnet crystals (YAG, GSGG, etc.) and also because of the polarized emission at the wavelength 1.06 μm that is a consequence of the anisotropic lattice of the ortho-vanadate hosts. That is why the Nd-doped ortho-vanadate lasers demonstrate in the continuous-wave regime a notable advantage over the ones based on the garnet crystals. Meanwhile, some drawbacks are met at the implementation of the PQS regime in the former lasers, at least, when the Q-switch is the YAG:Cr^{4+} crystal . The main problem in this sense is that the emission cross-section of, say, the Nd:YVO_4 crystal is too high such that is compatible with the low absorption cross-section of the YAG:Cr^{4+} saturable absorber (SA). It leads to a limitation of the energy stored in the active medium (AM) before a giant pulse (GP) is developing in the cavity. Thus, It is reflected in a relatively small pulse energy and peak power of the generated GP. It should be also noted that the pump power range where the PQS regime is supported in the Nd:YVO_4 / YAG:Cr^{4+} laser is strictly limited from the side of higher pump powers where the PQS mode is rapidly replaced, at the pump power increase, by the CW operation. Some measures were taken to overcome these problems, e.g., an implementation of the YAG:Cr^{4+}-switched lasers based either on new mixed ortho-vanadate AM like Nd:$Gd_iY_{1-i}VO_4$ with a decreased stimulated-emission cross-section, or an exploration of the lasers based on the standard Nd:YVO_4 crystals, but cut by a special manner . Another way to

implement the PQS Nd:YVO_4 laser is the use as a Q-switch unit of the LiF:F_2^- saturable absorber (SA) instead of the YAG:Cr^{4+} one. The absorption cross-section at the generation wavelength (1.06 μm) of LiF:F_2^- is higher than YAG:Cr^{4+}. Consequently, there is an effective operation of the Nd:YVO_4 / LiF:F_2^- laser; moreover, (and it is also important) there is a weakening of the demands to the intra-cavity focusing of the laser radiation in the switch; the latter makes the PQS regime stable within a much wider range of pump powers.

Motivation.

The principal aim of this thesis is to investigate the behavior and characteristics of a CW-pumped Nd:YVO_4 laser passively Q-switched with LiF:F_2^- or YAG:Cr^{4+} crystal, taking into account the geometric factor representing the distributions of the orientations of F_2^- color centers (relatively to the LiF host) and the Cr^{4+} ions (relatively to the YAG host) in order to know how this geometric factor influences the output parameters of the correspondent lasers (Nd:YVO_4/LiF:F_2- and Nd:YVO_4/ YAG:Cr^{4+}).

Overview of the thesis.

This thesis contains 5 chapters. Chapters 1 and 2 gives a brief theoretical description about the types of pumping in diode pumped lasers and Q-switching as well as the characteristics of the Nd:YVO_4 material used as active medium; chapters 3 and 4 describe the investigation and, consequently, the results obtained; in chapter 5 general conclusions of the investigation are shown. Finally an appendix is added where the publications and conferences derived of this work are presented.

Chapter 1. Diode Pumped Laser.

1.1 Diode pumping

The light source of pumped solid state lasers must supply the maximum possible light output in the spectral region that can be absorbed by the laser material. Electrical current, either continuous or pulsed, is supplied to the pump source and converted into optical radiation. The light source and laser material are contained in a pumping arrangement which concentrates the light from the pump source onto the laser material.

Today, only flashlamps, cw arc lamps and laser diodes are of practical interest. The most promising alternative to cw arc lamp and flashlamp pumping of solid-state lasers is the diode laser. The reason of the interest of this area stems from the dramatic increase in system efficiency, component lifetime and reduction of thermal load of the solid state material [1].

The laser diode pumping has many advantages that makes suitable for pumping Nd based solid state lasers. These advantages are shown next[2,3]:

- High pumping efficiency which stems for the high spectral overlap between the laser-diode emission and the Nd absorption bands at 808 nm.

- Laser diode arrays exhibit lifetimes on the order of 10^4 hrs., in CW operation and 10^9 shots in the pulsed mode.

- The directionality of diode radiation allows good spatial overlap between the pump radiation and low-order mode in the resonator.

- Weight and volume are reduced, besides not only are the laser pump sources small, but the laser resonator can be made small as well.

- Cooling requirements are reduced since the electrical efficiency of laser diodes is high.

On the other hand, there are some disadvantages for using laser diodes as pump sources. These are the following [4]:

- The cost of laser diodes is high, with a range from about ten dollars per watt for low-duty-cycle pulsed diodes in an array to as much as four hundred dollars per watt for cw lasers in a fiber coupled array in the case of 808-nm AlGaAs laser diodes. Other wavelengths may have different costs.

- The laser diode is very sensible to electro-static discharge and electrical transients. A short electrical spike will permanently damage a diode.

- The diode emission is not monochromatic, but has a bandwidth of 1nm for high power individual diodes and 2 to 4 nm for linear diode arrays.

- The output from a laser diode is not collimated but highly divergent, and for diode arrays it is multiaperture as well.

Typically two basic approaches have been followed in diode pumping of solid state lasers, namely end-pumping and side pumping configurations [5].

1.1.1 End pumping

End pumping configurations have the pump radiation collimated and focusing longitudinally into the laser material collinear with the resonator mode (fig. 1.1). Using a suitable focusing optics the pump radiation can be varied to coincide with the TEM_{00} resonator mode allowing the maximum use of energy from the laser diodes.

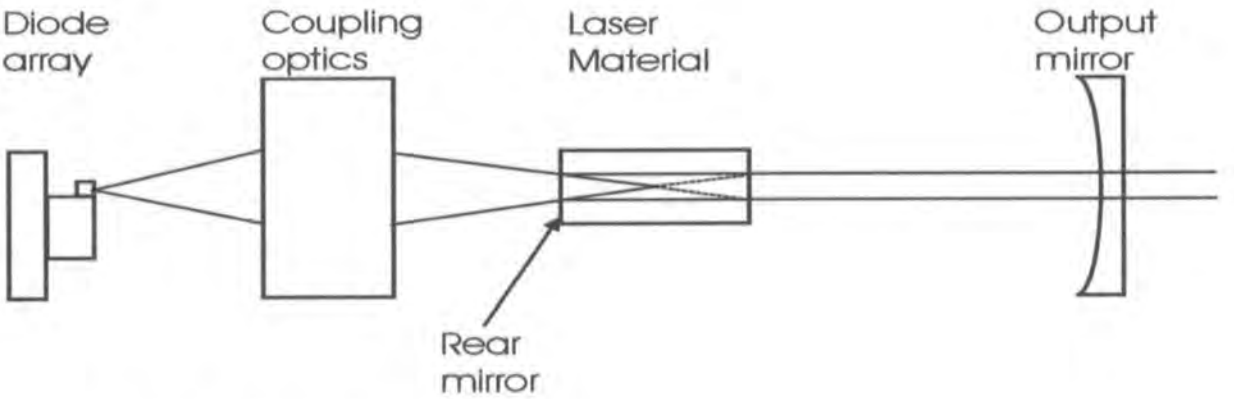

Fig. 1.1.- End pumping configuration

In its most basic form, end pumping involves a collimating lens with a large numerical aperture in order to collect radiation from a large cone angle, and a focusing lens to produce a small diameter spot inside the crystal. Since the radiation lobe emitted from a diode array has a high degree of astigmatism, one can introduce prism or cylindrical optics to transform the beam into a circular shape.

The high pump power density produces low-threshold and high slope efficiency operation, besides the absorption length can be as long as the crystal. In addition the optical conversion efficiency is high because the pump light can be deposited entirely within the fundamental mode volume.

Nevertheless, the power scaling by using fiber-coupled arrays is expensive, although the most practical approach. Moreover, the thermal management requirements are more severe for high-power end pumping, as energy deposition volumes tend to be small.

Finally, due to the high degree of alignment between the diode and the laser axis, laser light that leaks through the optical coating on the pumped face of the rod will be directed to the emitting facet of the diode causing a damage to the laser diode.

1.1.2. Side pumping.

In this configuration, the diode arrays are placed along the length of the laser rod or slab and pumped perpendicularly to the direction of propagation of the laser mode (fig 1.2). As more power is required, more diode arrays can be added along and around the laser rod. In some cases may not be required pump optics making it inexpensive. There is a reduction in the thermal load because the pumped volume in the rod is large.

There are some drawbacks in this configuration like it is more difficult to achieve a TEM_{00} operation. Pump efficiencies tend to be lower because a significant fraction of the pump energy is generally deposited outside the active volume.

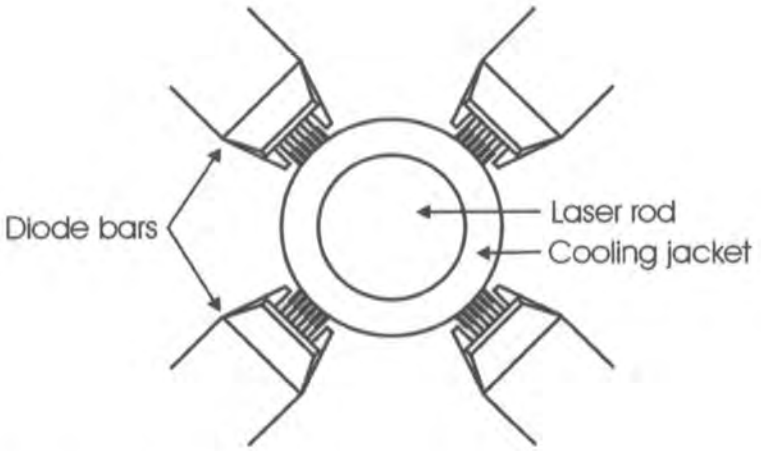

Fig. 1.2.- Side pumping configuration

1.1.2.1 Grazing incidence slab laser

The range of side-pumped geometries is far too extensive. One of side-pumped geometries which has attracted interest in recent days is the grazing incidence. In this case, a slab laser material is side pumped only in one face by means of a cylindrical lens (fig 1.3). Consequently, the resonator mode is located near the pumped face of the rod. Because of the use of laser materials with high absorption coefficient , the pump light does not penetrate deeply into the crystal in the direction transverse to the laser optical axis, experiencing a small region with high gain. The resonator mode makes a single grazing incidence total internal reflection at the pump face, thus remaining in the region of the highest gain throughout its passage through the slab. Using this geometry , 64 % conversion efficiency with a slope efficiency of 72% has been reported in high power systems [6].

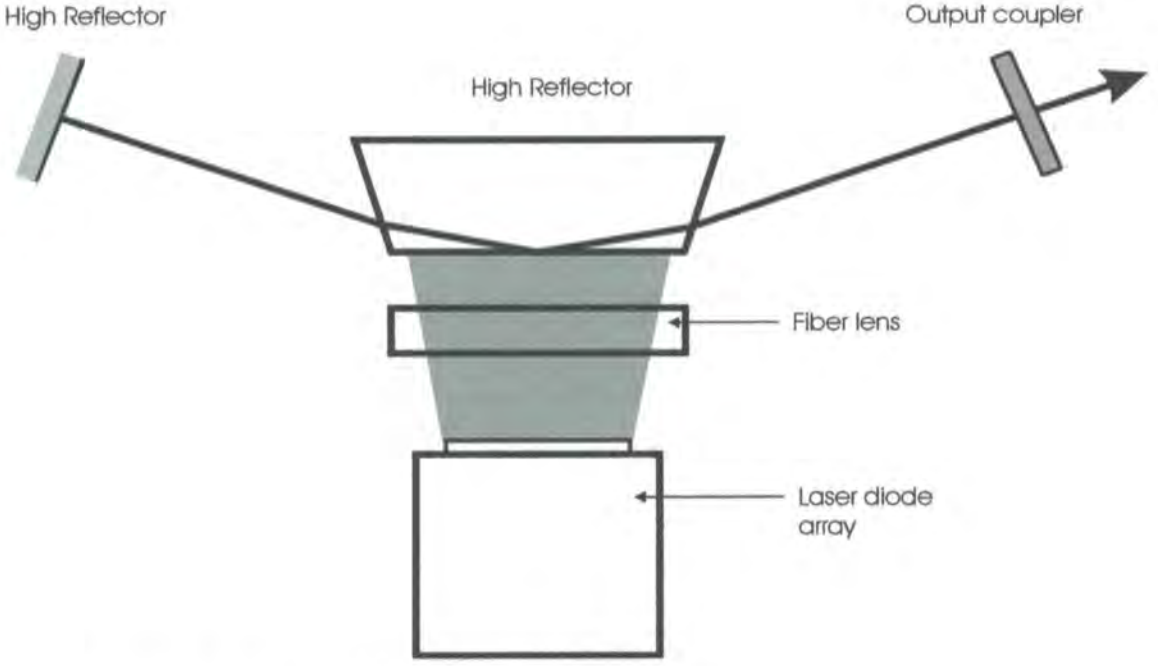

Fig. 1.3.- Grazing incidence slab laser

1.2 Active medium.

The active medium is responsible for the production of laser emission; it must have good optical, thermal and mechanical properties in order of being suitable for laser action. There are three well known host crystals that have characteristics desirable for diode pumping: YAG, YLF, and YVO_4.

1.2.1 Nd:YVO_4

Yttrium orthovanadate, YVO_4 , often referred to as "vanadate". Vanadate is a uniaxial crystal that produces a linearly polarized output [7]. This crystal combines the desirable properties of a large absorption bandwidth and high gain. The short fluorescence lifetime is an advantage for high repetition rate Q-switched laser operation. The properties of this crystal are summarized in table 1.1 [4].

Parameter	YVO_4
Crystal structure	uniaxial
τ_f (μs, 1% doping)	100
Thermal conductivity (W/cm K)	0.05
dn/dt (10^{-6} K^{-1})	8.5
Peak absorption wavelength (nm)	810
Absorption coefficient at peak (cm^{-1}, 1% doping)	41
Absorption bandwidth (FWHM, nm)	8
Knoop hardness (kg/cm^2)	480
Laser Wavelength (nm)	1.0641 (e) 1.0664 (o)
Linewidth (nm)	0.8
Refractive index at laser wavelength	2.168 (e) 1.958 (o)

Table 1.1. Host optical properties

References.

1. Tidwell, S.C., Seamans, J.F., Hamilton, C.E., Muller, C.H., and Lowenthal., Opt. Lett.,1991, **16**, 584

2. Yee Fan, T., and Byer R. L., 1988, IEEE J. Quant Electron., **24**, 895.

3. Koechner, W. "Solid State Laser Engineering", 4th ed., Springer Verlag , 1996.

4. Scheps, R. "Introduction to laser diode-pumped solid state lasers", SPIE ., 2001.

5. Yuan, G., Chong, T.C., and Xu B., 1998, Appl. Opt., **37**, 3971.

6. Damzen, M.J., Trew, M., Rosas, E., and Crofts, G.J., Opt. Commun., 2001,**196**, 237.

7. Cai, Z.P., Xu, H.Y., and Stéphan, G., Opt. Commun., 1997, **135**, 295.

Chapter 2. Q- switching

Q-switching is a widely used laser technique for the generation of short pulses of high intensity.[1] This technique allows to achieve a higher population inversion in the active medium delaying the laser action increasing the losses (low Q) inside the cavity. Then, after a large inversion is developed, the losses are reduced (high Q) producing a very short intense burst of laser output which dumps all the accumulated population inversion in a single short laser pulse, typically only a few tens of nanoseconds long.

There are many methods of Q-switching, which can be categorized in two groups: Active and Passive Q-switching.

2.1 Active

Active Q-switching inhibit the lasing action using external pulse sources or control circuitry .[2]

The standard methods of active Q-switching are the following:

- Rotating mirror Q-switching. This method consists in mounting the end mirror of the laser on a rapidly spinning motor shaft, therefore the laser action only takes place when the end mirror has an aligned orientation with respect to the opposite mirror (fig. 2.1).

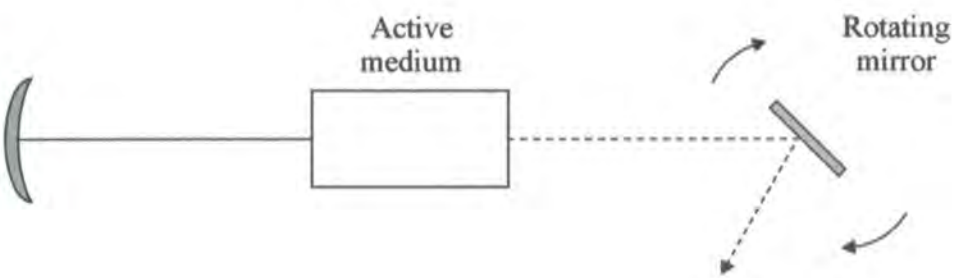

Fig 2.1.- Rotating mirror Q-switching

- Electrooptic Q-switching. An electrooptic modulator is used in this method and consist in an electrooptic crystal which becomes birefringent under the influence of an applied electrical voltage, besides one or more prisms or other polarizing elements inside the laser cavity. A voltage is applied to the pockels cell rotate the light 90° about the cavity axis therefore all the circulating energy is coupled out of the cavity by the polarizing element after just one trip. The low loss condition is reached torning the voltage off (fig. 2.2).

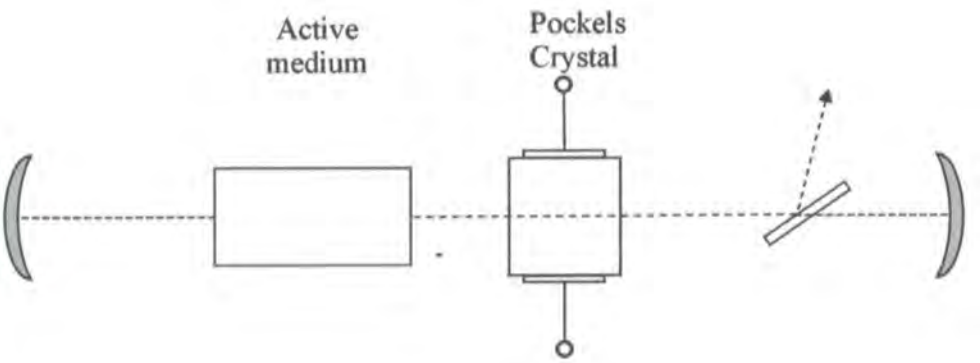

Fig 2.2.- Electrooptic Q-switching

- Acoustooptic Q-switching . An ultrasonic wave is launched into a block of transparent material producing a grating into the material. If a light beam is incident upon this grating, a portion of the intensity will be diffracted inhibiting the laser action (fig. 2.3).

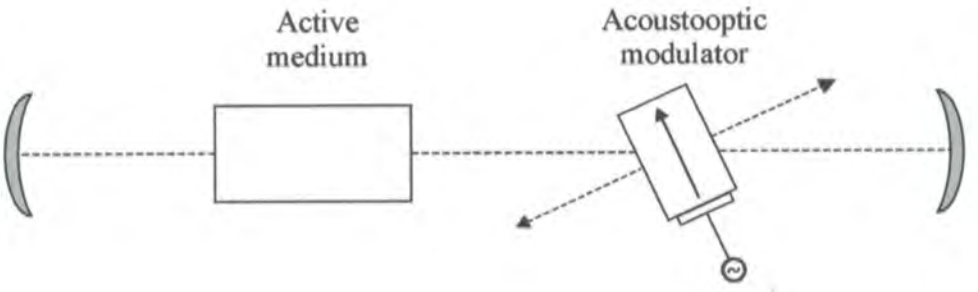

Fig 2.3.- Acoustooptic Q-switching

2.2 Passive.

The passive Q-switching method consists in a saturable absorber material inside the laser cavity. Laser inversion is built up by the pumping process until the gain inside the cavity exceeds this absorption and laser oscillation begins to develop inside the cavity. This oscillation at some relatively low level rapidly saturates the absorber and thus open up the cavity, lending to the development of a rapid and intense oscillation pulse.

Since the passive Q-switch is switched by the laser radiation itself it requires no high voltage, fast electro optic driver or RF modulation . The passive Q-switching has a simple design which leads to very small, robust a low cost systems.

Among the passive Q-switchers, Cr:YAG and LiF:F_2^- have shown good reliability and durability.

2.2.1 YAG:Cr^{4+}

YAG:Cr^{4+} is widely used as passive Q-switch in neodymium and ytterbium lasers because of its good photochemical and chemical stability, large absorption cross section, low saturating intensity, high thermal conductivity and high damage threshold [3,4].

One of the features of YAG:Cr^{4+} is the latent anisotropy of phototropic Cr^{4+} centers, which arises because of the ground state absorption saturation under the action of powerful resonant radiation. The latter is due to the resonantly absorbing dipoles orientation along the [1,0,0], [0,1,0] and [0,0,1] crystallographic axes of YAG as is show in fig. 2.5 [5,6,7].

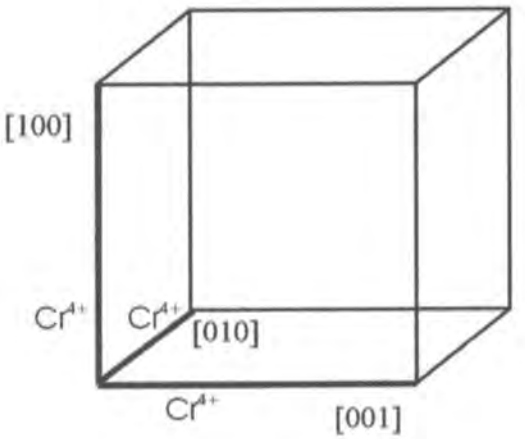

Fig 2.5.- Resonantly absorbing dipoles oriented along the YAG crystallographic axis.

2.2.2 LiF:F_2^-

Among the alkali halide crystals containing color centers, the LiF:F_2^- crystals are distinguished due to:

i) High thermal stability.

ii) High stability under infrared pumping radiation.

iii) High value of quantum efficiency of the luminescence[8].

F_2^- centers consist of a double vacancy configuration that shares three electrons[9] which are the responsible of the latent anisotropy of the crystal when they are resonantly saturated. These linear resonantly absorbing dipoles are oriented as is shown in fig. 2.5 in the LiF lattice[6].

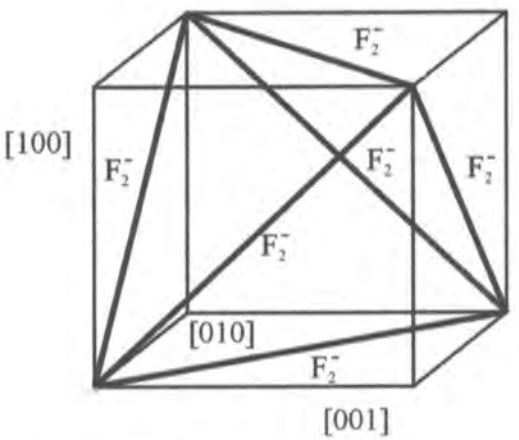

Fig 2.5.- F_2^- centers oriented along the LIF lattice.

References.

1. Siegman, A. E., "Lasers", University Science Books.

2. Koechner, W. "Solid State Laser Engineering," , 1996,4th ed., Springer Verlag.

3. Liu, J., Ozygus, B., Yang, S., Erhard, J., Seelig, U., and Weber, H., Meng, X., Zhu, L., Qin, L., Du, C., Xu, X., and Shao, Z., 2003, JOSA B, **20**, 652.

4. Choi, Y., 2001,Appl. Opt. ,**40**, 5417.

5. Eilers, H., Hoffman, K.R., Dennis, W.M., Jacobsen, S.M., and Yen, W.M., 1992, Appl. Phys. Lett., **61**, 2958.

6. Il'ichev, N.N., Kir'yanov, A.V., Pashinin, P.P., 1998, Quant. Electron., **28**, 147.

7. Brignon, A., 1996, JOSA B, **13**, 2154.

8. Basiev, T.T., Voron'ko, Y.K., Mirov, S.B., Osiko, V.V., Prokhorov, A.M., Soskin, M.S., and Taranenko, V.B., 1982, Sov. J. Quant. Electron., **12**, 1125.

9. De Rossi, W., Costa, F.E., Vieira Jr, N.D., Wetter, N., Morato, S.P., Basiev, T.T., Konyushkin, V.A., and Mirov, S.B. ,1992, Appl. Opt., **31**, 2719.

Chapter 3. Comparative analysis of passively Q-switched lasers.

3.1 Introduction.

CW-pumped Nd:YVO_4 lasers passively Q-switched with LiF:F_2^- and YAG:Cr^{4+} saturable absorbers are modeled and comparatively analyzed. The model used in this comparison takes into account the geometric factor representing the distributions of the orientations of the F_2^- color centers and Cr^{4+} ions relatively to the corresponding crystalline hosts on the output parameters of the lasers. It is shown that the LiF:F_2^- Q-switch has evident advantages over the YAG:Cr^{4+} one, in the senses of a much more expanded range of pump powers where the giant-pulse regime is supported in the laser and, as the consequence, of potentially higher average output and peak pulse powers accessible.

3.1 Model.

A schematic sketch of a longitudinally-diode-pumped Passive Q-Switching (PQS) Nd:YVO_4 laser is shown in Fig.3.1.

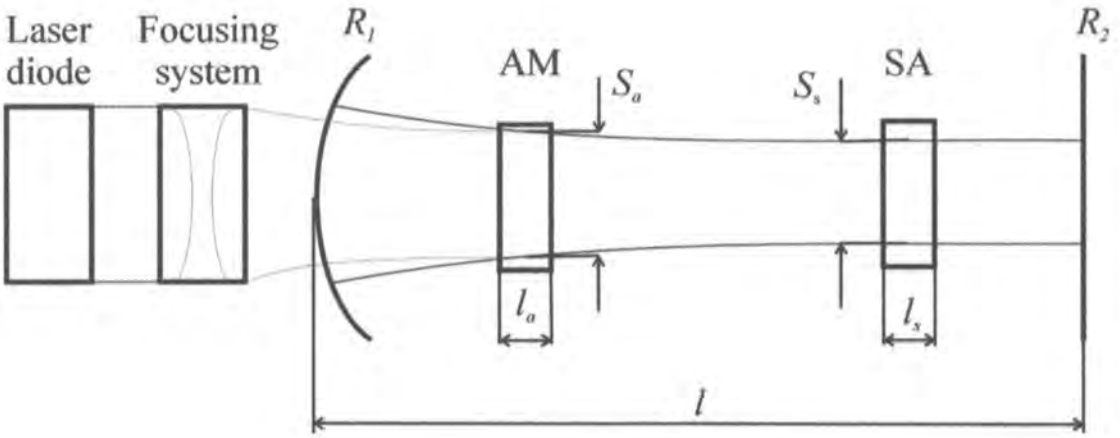

Fig.3.1. Arrangement of Nd:YVO_4 laser passively Q-switched with YAG:Cr^{4+} or LiF:F_2^- SA.

The cavity consists of a pair of mirrors surrounding a Nd:YVO_4 crystal used as active medium (AM) and a LiF:F_2^- or YAG:Cr^{4+} crystal used as saturable absorber (SA). It is supposed that there are no additional elements in the cavity, since the role of a diaphragm is played by the longitudinally-pumped area within the active element which effectively selects the transversal modes and the role of a polarizer – by the c-cut Nd:YVO_4 AM itself, being a highly polarizing optical material[1].

The PQS laser dynamics is governed by the following rate equations:

$$\frac{dF_a}{dt} = \frac{F_a}{t_R}\left[2\sigma_a N_a l_a - 2\sigma_s l_s \sum_i^M n_s^{(i)} \left(\vec{a_i}\vec{e_0}\right)^2 - \ln\left(\frac{1}{r}\right) - \alpha\right] + k\frac{N_a}{\tau_a}, \tag{3.1}$$

$$\frac{dN_a}{dt} = -\gamma\sigma_a N_a F_a c - \frac{N_a}{\tau_a} + R_p, \tag{3.2}$$

$$\frac{dn_s^{(i)}}{dt} = -\sigma_s \left(\vec{a_i}\vec{e_0}\right)^2 n_s^{(i)} F_a c K + \frac{n_s^0 - n_s^{(i)}}{\tau_s}, \qquad i = 1 \div M, \tag{3.3}$$

where the variables are as follows: F_a, the average photon density inside the cavity; N_a, the population inversion in AM; and $n_s^{(i)}$, the ground state populations of the Cr^{4+} ions of the *i*-orientation relatively to the YAG lattice (M=3 [2,3]), see Fig.3.2 (a), or F_2^- color centers of the *i*-orientation relatively to the LiF lattice (M=6 [4,5]), see Fig.3.2 (b).

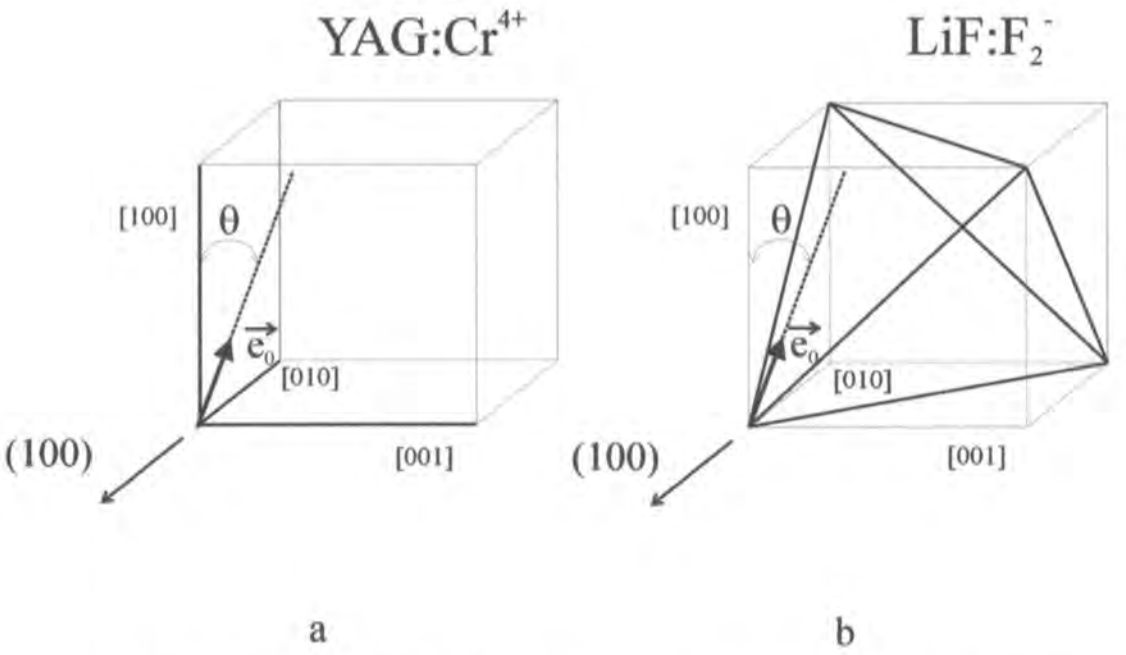

Fig.3.2. Arrangements of interaction of intra-cavity generation wave (with polarization azimuth given by vector $\boldsymbol{e_0}$) with resonantly absorbing dipoles ($\boldsymbol{a_i}$, $i = 1 \div M$), which are Cr^{4+} ions (YAG: Cr^{4+} SA, $M = 3$) (a) and F_2^- centers (LiF:F_2^- SA, $M = 6$) (b).

The parameters entering the equations are: σ_a, the AM lasing cross-section; σ_s, the Cr^{4+}:YAG / LiF:F_2^- resonant absorption cross-section caused by the dopants in SA (i.e., the F_2^- color center and Cr^{4+} ion); l_a and l_s, the lengths of AM and SA, respectively; $K = S_a/S_s$, the ratio of the transverse area of the laser beam in AM to that in SA; r, the reflection coefficient of the output mirror (useful loss); $\alpha = \alpha_0 + \beta_0$, the overall non-resonant losses (composed of the passive cavity loss α_0 and the loss $\beta_0 = -ln(T_{fin})$ owing to the incomplete bleaching of SA at high intensities, where T_{fin} is the full-bleached transmission coefficient of SA); γ, the AM population inversion reduction factor [6]; t_R, the round-trip time of light in the cavity of the optical length L ($t_R = 2L/c$; $L = l + l_a m_a + l_s m_s$, where m_a and m_s are the effective refractive indices of the YVO_4 and YAG / LiF hosts, respectively, and c is the

velocity of light); τ_a and τ_s, the relaxation times of the Nd:YVO_4 AM population inversion and Cr^{4+}:YAG / LiF:F_2^- SA excited-state, respectively; k, the factor accounting for the spontaneous radiation in the laser mode; and R_p, the volumetric pump rate.

The two important parameters of the model are n_s^0, the initial (non-disturbed) ground-state populations of the dopants in SA (the Cr^{4+} ions and F_2^- color centers) and N_a^{in}, the initial (threshold) value of the population inversion in the Nd:YVO_4 AM.

The non-disturbed dopant's populations are determined as follows:

$$n_s^0 = \frac{\alpha_s^0}{\sigma_s \sum_i^M \left(\vec{a_i}\vec{e_0}\right)^2} = -\frac{\ln\left(\frac{T_{in}}{T_{fin}}\right)}{\sigma_s l_s \sum_i^M \left(\vec{a_i}\vec{e_0}\right)^2} = -\frac{3\ln\left(\frac{T_{in}}{T_{fin}}\right)}{\sigma_s l_s M}, \tag{3.4}$$

where: α_s^0 is the resonant absorption coefficient of SA, T_{in} is the initial (weak-signal) transmission coefficient of SA at the wavelength 1.06 μm. In formula (3.4), $\boldsymbol{a_i}$ are the unit vectors for the dopant centers considered as linear resonantly absorbing dipoles and $\boldsymbol{e_\theta}$ is the unit vector coinciding with the polarization azimuth of a generation wave, circulating in the cavity (which, in turn, is dictated by the orientation of the Nd:YVO_4 active crystal). Note that because of the presence in a SA centro-symmetric crystal host of the few groups of resonantly absorbing dipoles oriented definitely (by the $\boldsymbol{a_i}$ vectors, see Fig.3.2), the sum $\sum_i^M F_i(\theta) = \sum_i^M \left(\vec{a_i}\vec{e_0}\right)^2$ is equal to M/3 for any distribution of these orientations at the thermo-dynamical equilibrium. Thus, the functions $F_i(\theta)$ address the "geometric factor" of a

particular distribution of the phototropic dopant centers in the sample and therefore is connected with the latent anisotropy of the doped crystal (the angle θ counts the current angular coordinate of the generation wave polarization azimuth with respect to one of the main crystallographic axes of SA, see Fig.3.2). The last feature does cause the peculiarities of the self-induced resonant-absorption anisotropy in a doped crystalline SA [2-5].

The initial value of the population inversion in the Nd:YVO_4 AM, N_a^{in}, is defined as:

$$N_a^{in} = \frac{\alpha + \ln\left(\frac{1}{r}\right) - \ln\left(\frac{T_{in}}{T_{fin}}\right)}{2\sigma_a l_a}, \qquad (3.5)$$

Note that formula 3.5 is obtained neglecting the last term in Eq.(3.1), which answers to the contribution of the spontaneous emission in the laser mode, so that the N_a^{in} parameter does not depend, as the direct calculations show, on the nonlinear anisotropic properties of SA.

It is clear that the presence of the functions $F_i(\theta)$ in Eqs.(3.1) and (3.3) makes the laser model represented by the system (3.1)-(3.3) essentially sensitive to the self-induced anisotropy appeared in SA on the nonlinear stage of a GP's formation. This holds for any position of either a LiF:F_2^- or YAG:Cr^{4+} crystal relatively to the orientation of a Nd:YVO_4 crystal, which, as it was mentioned above, dictates the (linear) state of polarization established in the laser. (Note that for the anisotropic Nd:YVO_4 AM the generation wave's

polarization is fortunately fixed through the lasing cycle, so the nonlinear polarization rotation effect observed in the lasers based on the Nd-garnet AM [7,8] is fully eliminated).

To make the further analysis simpler, let us specify that the cuts of both the LiF and YAG crystalline hosts are positioned in the cavity as (100), so the light propagates along their [100]-like crystallographic axis, while the laser polarization azimuth (given by the orientation of the Nd:YVO_4 AM) is kept fixed and, of course, orthogonal to this direction.

We were interested in numerical calculations of the system (3.1)-(3.3) performed for the different orientations of the LiF:F_2^- or YAG:Cr^{4+} crystals inside the cavity. It is easily to show that the geometric factors $F_i(\theta)$ are, e.g.,

$$F_1(\theta) = \cos^2(\theta), \tag{3.6a}$$

$$F_2(\theta) = \sin^2(\theta), \tag{3.6b}$$

$$F_3(\theta) \equiv 0 \tag{3.6c}$$

for the (100)-cut YAG:Cr^{4+} SA (Fig.3.2(a)) and

$$F_1(\theta) = \frac{1}{2}[\sin(\theta) + \cos(\theta)]^2, \tag{3.7a}$$

$$F_2(\theta) = F_3(\theta) = \frac{1}{2}\cos^2(\theta), \tag{3.7b}$$

$$F_4(\theta) = F_5(\theta) = \frac{1}{2}\sin^2(\theta), \tag{3.7c}$$

$$F_6(\theta) = \frac{1}{2}[\sin(\theta) - \cos(\theta)]^2 \tag{3.7d}$$

for the (100)-cut LiF:F_2^- SA (Fig.3.2 (b)).

Finally, the pump volumetric rate, R_p, is calculated using the following relationship:

$$R_p = \frac{P\left(1-e^{-\Lambda_a l_a}\right)}{S_p l_a h\nu_p \frac{\lambda_p}{\lambda_g}}, \tag{3.8}$$

where: P is the longitudinally-launched diode pump power, $S_p l_a$ is the AM pumped volume, and λ_p/λ_g is the Stokes-loss parameter given by the pump-to-generation wavelength ratio [9]. Note that because of a huge absorption coefficient Λ_a of Nd:YVO_4 at the pump wavelength, the expression in brackets is practically equal to 1 (in other words, the pump power P is whole-absorbed within the active crystal).

Eqs.(3.1-3.8) are numerically calculated, allowing one to obtain the main characteristics of the Nd:YVO_4 lasers with the YAG:Cr^{4+} or LiF:F_2^- SA, i.e., the range of pump powers where the PQS regime is supported and the laser basic parameters - GP energy, duration, and peak power, repetition rate of GPs in a train, and laser average output power.

3.1 Results and discussion.

Since the problem (3.1)-(3.8) involves many parameters to be varied, we have stopped on an analysis of the most general scheme of a mini-Nd:YVO_4 laser with a (100)-cut YAG:Cr^{4+}, or LiF:F_2^- SA (Fig.3.1), where the variables are only (i) the angular position (θ) of each of the switches relatively the polarization direction set by the Nd:YVO_4 AM and (ii) the focusing parameter K, accounting for the ratio of the transverse areas of the laser beam in AM and SA, which is given by the curvature radii of the mirrors composing the cavity. All other parameters have been fixed as follows:

Nd:YVO_4 AM: c-cut, $A_a = 30.0\ cm^{-1}$, $N_{tot} = 1.5 \times 10^{20}\ cm^{-3}$, $\sigma_a = 2.1 \times 10^{-18}\ cm^2$, $\gamma = 1.0$, $\tau_a = 100 \times 10^{-6}$ s, $S_a = 2.0 \times 10^{-3}\ cm^2$, $m_a = 2.06$, $l_a = 1.0$ cm;

LiF:F_2^- SA: (100)-cut, $M = 6$, $\sigma_s = 1.3 \times 10^{-17}\ cm^2$, $\tau_s = 0.1 \times 10^{-6}$ s, $m_s = 1.37$, $l_s = 0.8$ cm, $T_{in} = 90\%$, $T_{fin} = 99\%$;

YAG:Cr^{4+} SA: (100)-cut, $M = 3$, $\sigma_s = 5.6 \times 10^{-18}\ cm^2$, $\tau_s = 4.0 \times 10^{-6}$ s, $m_s = 1.82$, $l_s = 0.15$ cm, $T_{in} = 90\%$, $T_{fin} = 99\%$;

Laser cavity: $l = 10$ cm (giving the total optical cavity length $L \approx 13$ cm), $\alpha_0 = 0.01$, $R_1 = 100\%$, $R_2 = 95\%$;

Other parameters: generation - $\lambda_g = 1.06 \times 10^{-4}$ cm (quanta energy $h\nu_g = 1.85 \times 10^{-19}$ J), pump - $\lambda_p = 0.808 \times 10^{-4}$ cm (quanta energy $h\nu_p = 2.45 \times 10^{-19}$ J), $k = 10^{-4}$, $c = 3 \times 10^{10}$ cm, $t_R \approx 0.85 \times 10^{-9}$ s.

The total non-resonant intra-cavity losses are $\alpha = \alpha_0 + \beta_0 = 0.02$ (where $\beta_0 = -ln(T_{fin}) = 0.01$), providing the same start conditions for lasing. Therefore, the initial (threshold) value of the population inversion in AM is (according to formula (3.5)) $N_a^{in} = 3.97 \times 10^{16}$ cm^{-3} (for either SA), and the non-disturbed Cr^{4+} (YAG:Cr^{4+} SA) and F_2^- (LiF:F_2^- SA) dopant's ground-state populations are (according to formula (3.4)) $n_s^0 = 1.14 \times 10^{17}$ cm^{-3} and 4.58×10^{15} cm^{-3}, respectively. At last, we take for simplicity that the geometrical cross-sections of the pump and generation waves inside the Nd:YVO_4 AM are the same: $S_p = S_a$.

The modeling results are shown in figs.3.3 to 3.7.

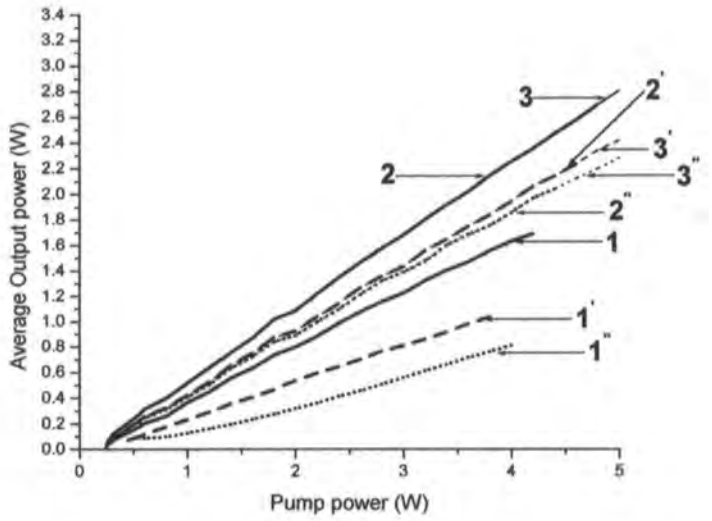

(a)

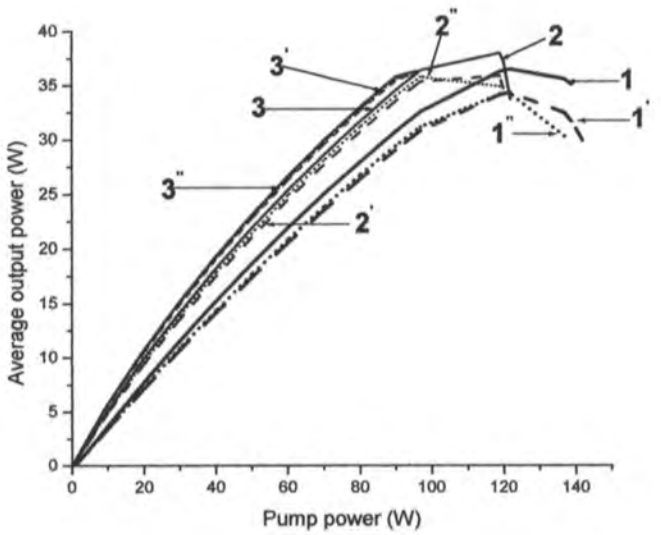

(b)

Fig.3.3. Dependences of average power of Nd:YVO_4 laser Q-switched with YAG:Cr^{4+} (a) and LiF:F_2^- (b) SA versus pump power.

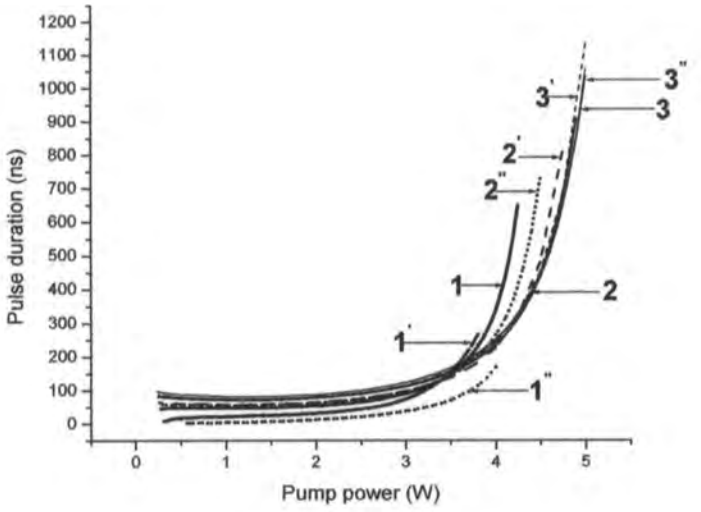

(a)

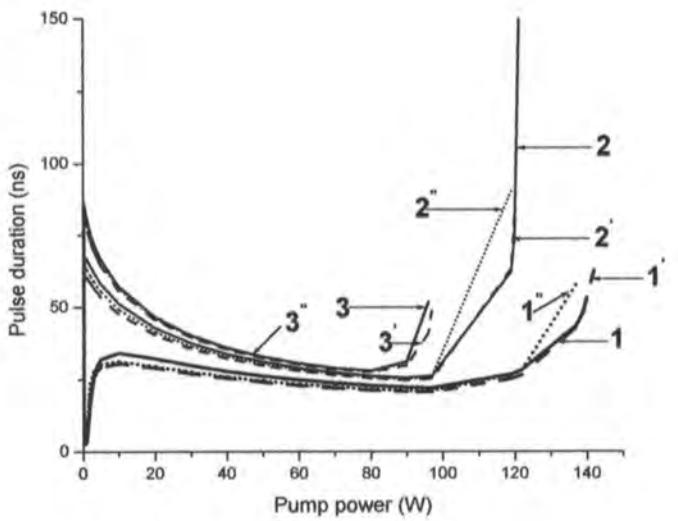

(b)

Fig.3.4. Dependences of pulse duration of Nd:YVO_4 laser Q-switched with YAG:Cr^{4+} (a) and LiF:F_2^- (b) SA versus pump power.

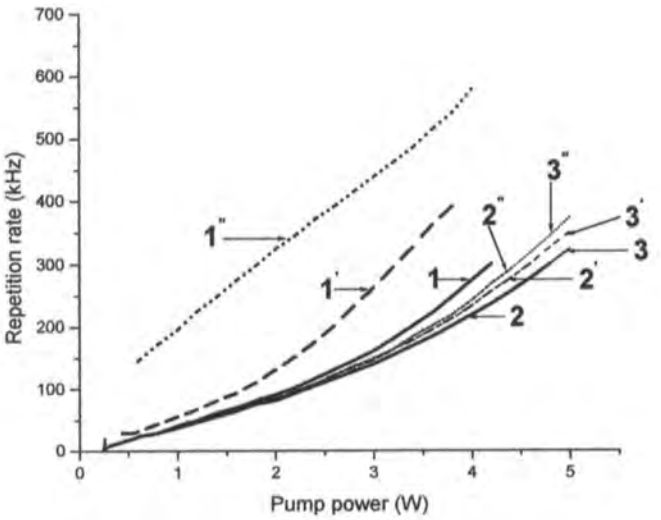

(a)

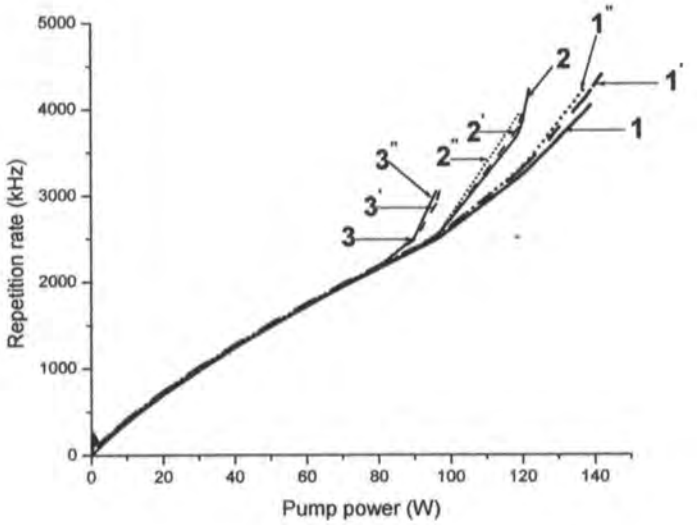

(b)

Fig.3.5. Dependences of repetition rate of Nd:YVO_4 laser Q-switched with YAG:Cr^{4+} (a) and LiF:F_2^- (b) SA versus pump power.

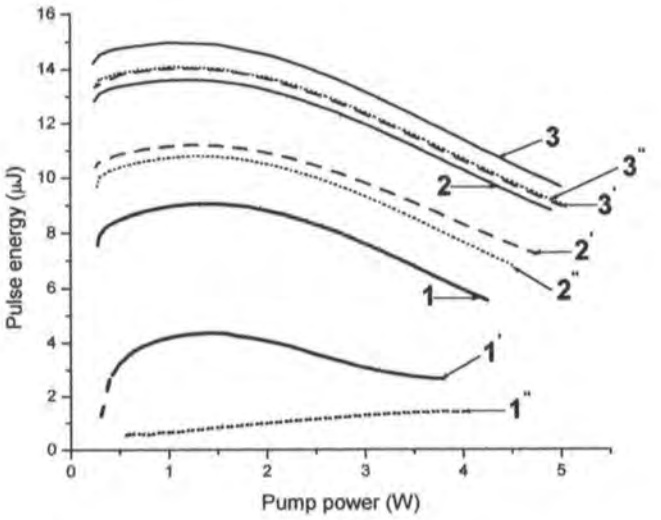

(a)

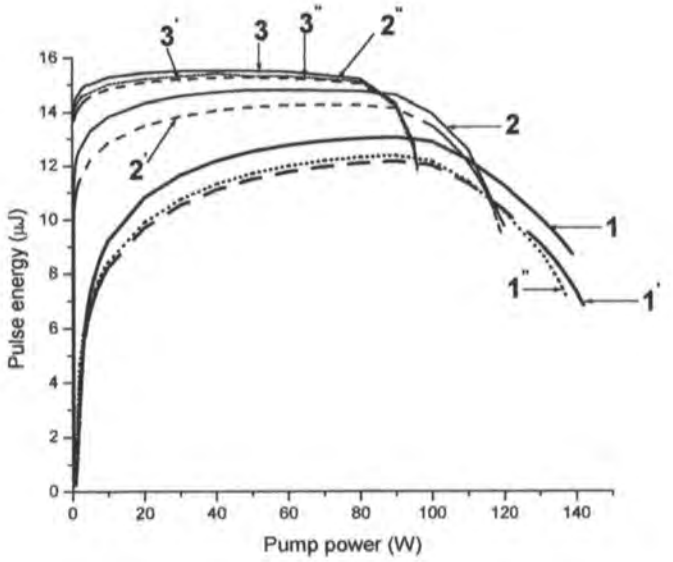

(b)

Fig.3.6. Dependences of pulse energy of Nd:YVO_4 laser Q-switched with YAG:Cr^{4+} (a) and LiF:F_2^- (b) SA versus pump power.

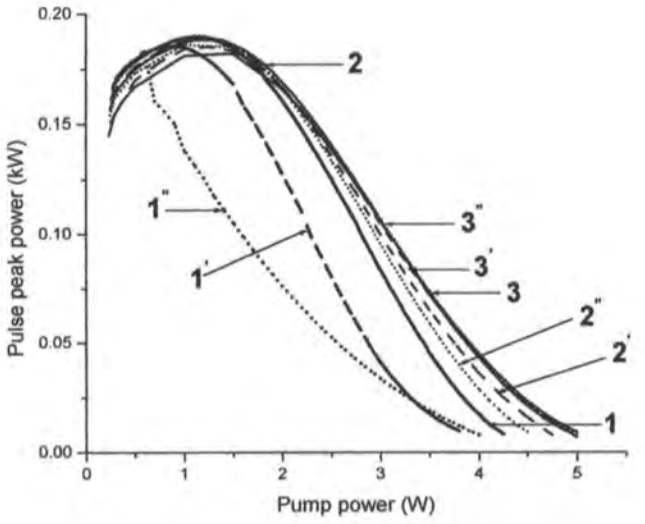

(a)

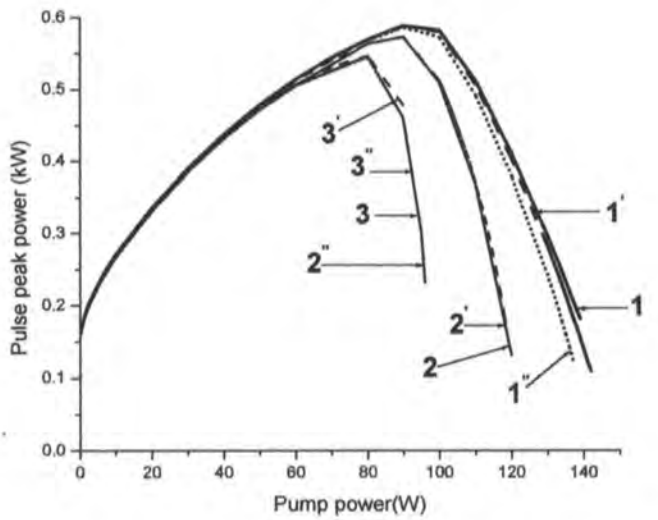

(b)

Fig.3.7. Dependences of pulse peak power of Nd:YVO_4 laser Q-switched with YAG:Cr^{4+} (a) and LiF:F_2^- (b) SA versus pump power.

In all the graphs, the dependences of the basic laser parameters (average output power, repetition rate of pulses in a train, and duration, energy, and peak power of a separate GP) are plotted versus pump power P, where the graphs labeled (a) relate to the YAG:Cr^{4+} SA and the graphs labeled (b) – to the LiF:F_2^- SA. In these plots are given the results of the calculations proceeded for the different orientations θ (θ = 0°, 22.5°, and 45° with respect to the polarization set in the laser) of either SA and also for the different relative focusing parameters K (K = 0.8, 2, and 5) where curves 1 (θ = 0°), 1' (θ = 22.5°) and 1'' (θ = 45°) correspond to K=0.8; curves 2 (θ = 0°), 2' (θ = 22.5°) and 2'' (θ = 45°) correspond to K=2; curves 3 (θ = 0°), 3' (θ = 22.5°) and 3'' (θ = 45°) correspond to K=5. The set of results (figs. 3.3-3.7) gives a comprehensive illustration of the processes occurring in the laser and the differences in the regimes appeared owing to the use as a SA of either the YAG:Cr^{4+}, or LiF:F_2^- crystal.

The main deductions from figs.3.3 to 3.7 are as follows:

(i) The PQS regime in the Nd:YVO_4 laser is obtained in a considerably wider range in the case the LiF:F_2^- crystal compared to the case of the YAG:Cr^{4+} crystal . The upper limits of the PQS regimes' stability are, respectively, ~120 W and ~5 W. At the same time, the threshold power in both cases is the same, which is determined by the same value of all the cavity linear parameters as well as the same chosen values of the weak-signal and whole-bleached transmittances of the switches (that is why the threshold population inversion N_a^{in} in the Nd:YVO_4 AM is also the same in either case, see formula 3.5).

(ii) Correspondingly, the maximum average output powers for the PQS regime are, respectively, ~3 W (YAG:Cr^{4+} SA) and ~35 W (LiF:F_2^- SA), see fig.3.3. A direct consequence of this feature is that the attainable values of the GPs' peak power are: ~0.2 kW (YAG:Cr^{4+} SA) and ~0.6 kW (LiF:F_2^- SA), see fig.3.7.

(iii) Generally to say, the dependences of all the laser output parameters are less sensitive to the angular position θ of the LiF:F_2^- SA rather than those of the YAG:Cr^{4+} SA. This is a consequence of the fact that the case of six equivalent resonantly absorbing dipoles (LiF:F_2^- SA, see fig.3.2(b)) results in a less-pronounced nonlinear-absorption anisotropy effect than the case of three dipoles (YAG:Cr^{4+} SA, see fig.3.2(a)) does.

(iv) The laser PQS with the YAG:Cr^{4+} SA is more sensitive to the intra-cavity focusing arrangement (i.e., to the *K*-parameter) than the laser PQS with the LiF:F_2^- SA. So, the former laser always needs a more tight focusing of the laser beam in the switch, that sometimes is a drawback (an increase of the *K*-parameter inevitably results in a narrowing of the pump power range where the PQS mode sets).

(v) The maximum GP energy and minimum pulse width for both the lasers are virtually the same - ~15 μJ and ~25 ns, respectively (compare fig.3.4 and fig.3.6). Meanwhile, the most "integral" parameter of either laser is the repetition rate of GPs in a CW train: E.g., in the case of the LiF:F_2^- SA, neither the angular position θ of the crystal, nor the focusing strength (given by K) reflects pronounceably on the repetition rate in a whole accessible range of pump powers (see fig.3.5).

Let us give more physical explanations for some of the above conclusions, which are quite surprising on the first view, but are simply explained indeed. First of all, the LiF:F_2^- crystal has a significantly higher resonant absorption cross-section at the lasing wavelength than has the YAG:Cr^{4+} one (1.3×10^{-17} and 5.6×10^{-18} cm^2, respectively); therefore the demands for a tight focusing of the generation radiation in the switch for getting the PQS regime are essentially weaker for the first SA. By the same time, the saturating intensities (i.e., the intensity at which the resonant absorption of a doped crystal is bleached),

$$I_S \propto \frac{h\nu_g}{\sigma_s \tau_s}, \qquad (3.9a)$$

are strongly differed for YAG:Cr^{4+} and LiF:F_2^- (16.5 and 142 kW/cm^2, respectively). Therefore, it is understandable why the PQS regime in the case of the LiF:F_2^- SA has a much higher pump power limit than that in the case of the YAG:Cr^{4+} SA. However, the

ratio I_S (LiF:F_2^-) / I_S (YAG:Cr^{4+}) ≈ 8.5 does not fully explain the difference in the pump power ranges, where the PQS regime is, according to the modeling results (Figs.3.3÷3.7), supported in these two cases: For instance, at K = 5, this range for the YAG:Cr^{4+} SA is limited by ~ 5 W, whereas for the LiF:F_2^- SA it is limited by ~ 125 W, so the difference of the pump power ranges is ≈ 25, i.e. about 3 times more !

Meanwhile, the last fact is perfectly explained in the frames of our model. The explanation re-calls the geometrical factor representing the distributions of the orientations of the F_2^- color centers in LiF and the Cr^{4+} ions in YAG. Indeed, since in the case of the YAG:Cr^{4+} SA, the absorptions of only two groups of the resonant dipoles (Cr^{4+} ions, see fig.3.2(a)) lying in the plane orthogonal to the propagation of the generation wave in the cavity are of the sense. Therefore, the crystal's transmittance quite rapidly approaches the fully-saturated value, where any source of self-pulsing in the laser disappears and the PQS regime is replaced by the CW operation. The saturation occurs in a sequence, dictated by the "efficiency" of interaction of these two Cr^{4+} ion groups with the intra-cavity 1.06-μm radiation (the third group does not interact with the generation wave at all, being parallel to its propagation direction); the corresponding saturating intensities I_S are:

$$I_s^{\begin{bmatrix}1\\2\\3\end{bmatrix}}(\theta) \propto \frac{h\nu_g}{\sigma_s\tau_s \begin{bmatrix}\cos^2(\theta)\\ \sin^2(\theta)\\ 0\end{bmatrix}} \qquad (3.9b)$$

(see formulas 3.6). E.g., for the YAG:Cr^{4+} SA oriented by the angle $\theta = 22.5°$, $I_S^{[1]} \approx 9.7$ kW/cm^2 and $I_S^{[2]} \approx 56.4$ kW/cm^2. (It is also evident that for $\theta = 0°$ and 90° only single Cr^{4+} ion groups are bleached, whereas for $\theta = 45°$ the two groups are bleached with the same "efficiency").

Alternatively, in the case of the LiF:F_2^- SA, the picture, being similar in the physical sense, is more complicated at the appearance. Now, I_S may be written analogously to the above estimate (3.9(b)) with the use of formulas (3.7) as:

$$I_s^{\begin{bmatrix}1\\2\\3\\4\\5\\6\end{bmatrix}}(\theta) \propto \frac{h\nu_g}{\sigma_s\tau_s \begin{bmatrix} \frac{1}{2}[\sin(\theta)+\cos(\theta)]^2 \\ \frac{1}{2}\cos^2(\theta) \\ \frac{1}{2}\cos^2(\theta) \\ \frac{1}{2}\sin^2(\theta) \\ \frac{1}{2}\sin^2(\theta) \\ \frac{1}{2}[\sin(\theta)-\cos(\theta)]^2 \end{bmatrix}}; \qquad (3.9c)$$

therefore, the existence of six equivalent resonant F_2^- color-center groups in LiF leads to the presence (in the geometry shown in Fig.3.2(b)) of the four saturating intensities - $I_S^{[1]}$, $I_S^{[2]} = I_S^{[3]}$, $I_S^{[4]} = I_S^{[5]}$, and $I_S^{[6]}$, which, e.g., for the orientation $\theta = 22.5°$, are ≈ 166.7, 333.4, 1943.1, and 971.7 kW/cm^2. It means that the six groups of the F_2^- centers interact now with

the intra-cavity radiation with the different "efficiencies" – so that each group is effectively bleached in a sequence at the increase of pump power. It is interesting to note that the ratio between the maximum of the listed saturating intensity for the LiF:F_2^- SA and the one for the YAG:Cr^{4+} SA is about 30-35 because it can explain the ratio 25-30 observed between the maximum pump power accessible for the PQS regime supported in the laser with the YAG:Cr^{4+} and LiF:F_2^- SA (see above)

Some additional evidences for the formulated conclusions stem from figs.3.8 and 3.9, where a few portraits of CW-trains of GPs and the corresponding "snapshots" of the temporal behavior of the ground-state populations of F_2^- color centers in LiF (fig.3.9) and Cr^{4+} ions in YAG (fig.3.8) are shown. These graphs have been numerically calculated for the same orientation of the switches ($\theta = 22.5^\circ$) and for the two values of pump power – 5 W (the Nd:YVO_4 / YAG:Cr^{4+} laser) and 5 and 50 W (the Nd:YVO_4 / LiF:F_2^- laser). One can easily deduce that the resonant-absorption bleaching is everywhere different for the differently oriented centers, being a source of the features annotated above.

Note that the discussed analysis of the Nd:YVO_4 laser with the YAG:Cr^{4+} and LiF:F_2^- SAs addresses only the characteristics stemming from the effect of intensity-dependent transmittance in these SA, which allows one to roughly model the laser. In a real laser, many other effects, which are not covered by the present analysis, act. Let us mention some important of them, which would have an impact on the laser operation :

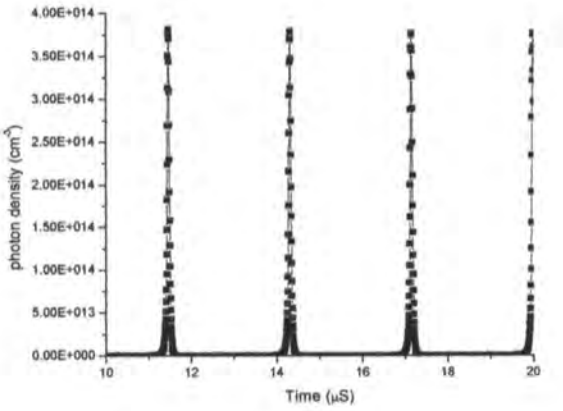

(a)

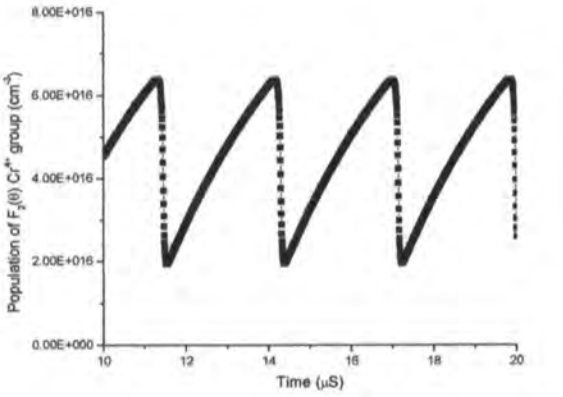

(b)

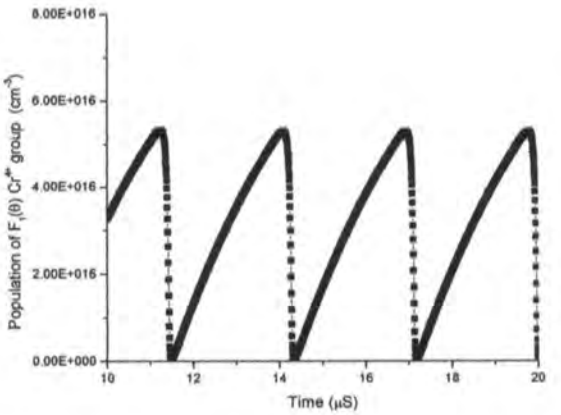

(c)

Fig.3.8. Train of GPs (a) and correspondent snapshots (b-c) of ground-state populations of three groups of Cr^{4+} ions (YAG:Cr^{4+}) versus time. $\theta = 22.5°$; $K = 2$; $P = 5$ W.

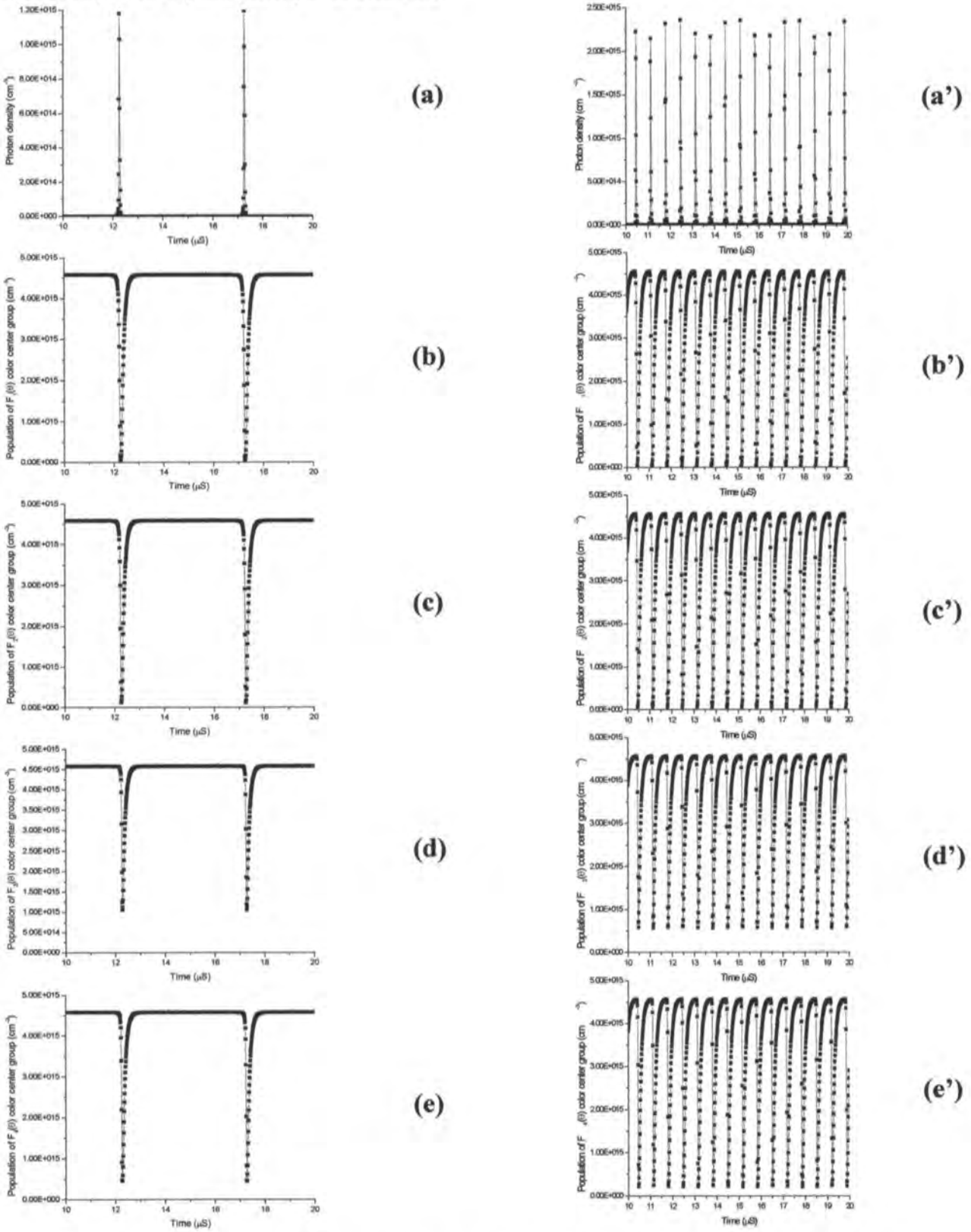

Fig.3.9. Trains of GPs (a, a') and correspondent snapshots (b-e, b'–e') of ground-state populations of six groups of F_2^- centers ($LiF:F_2^-$) versus time. $\theta = 22.5°$; $K = 2$; $P = 5$ W (a–d) and 50 W (a'–d').

(1) *The excited-state absorption (ESA) in SA.* For both the crystals (YAG:Cr^{4+} and LiF:F_2^-), there are the evidences for the presence of the ESA at the lasing wavelength (1.06 μm). It should be quite straightforward to take into account this effect as ESA plays a role of additional losses in the cavity and may be easily incorporated in the model [10,11]. We did not perform here the ESA-effect modeling, since it complicates the analysis and results in a loose of clarity; in addition, there is no any data concerning the anisotropic properties of the ESA in either of the YAG:Cr^{4+} and LiF:F_2^- crystals. One more appearance of the ESA-effect in the YAG:Cr^{4+} and LiF:F_2^- crystals is that the ESA leads, at some arrangement of the cavity, to the self-mode-locking effect [12,13,14,15,16] which is represented as a modulation of the GPs at the frequency of the longitudinal modes' beating. The last effect comes out the present paper' scope.

(2) *The laser nonlinear-dynamics features.* As it has been reported in [17], the Nd:YVO_4 / YAG:Cr^{4+} laser at high pump powers demonstrates all the properties of an autonomous class-B laser, i.e., the appearance of multiple attractors, bifurcations, transition to chaos, etc. Most probably, of a similar behavior should be the Nd:YVO_4 / LiF:F_2^- laser, too. However, a thorough comparison of the latter phenomena in these two lasers needs a separate investigation.

(3) *The thermo-induced effects in AM and SA.* These effects have a big impact on the work of a CW-pumped PQS Nd-laser. At high pump powers, these effects shall be inevitably switched on in a Nd:YVO_4 AM [18,19], and either YAG:Cr^{4+} or LiF:F_2^- SA [6,20-22] and have to be accounted for at the real laser's modeling. Note here that a possible consequence of the thermo-induced effects, apart from the evident influence on the cavity stability at the high pumps, is the appearance of the characteristic frequencies (of the kHz-range) in the RF- spectrum, corresponding to the times of thermal relaxation in the AM and SA. The last feature may additionally disturb the PQS regime – there would appear pronounceable instabilities of the GPs' amplitude and jitter.

(4) *The pump-induced bleaching effect in SA.* As it has been shown recently [23], some role in the establishing of the PQS in the Nd:YVO_4 / YAG:Cr^{4+} laser is played by the extra-bleaching effect in the SA under the influence of non-filtered (or not whole-absorbed by the AM) radiation of the pumping diode laser. We neglect this effect in the present report, implying that in the case of the Nd:YVO_4 AM set in the cavity between the pumping diode laser and either SA (fig.3.1), the pump-induced extra-bleaching is negligible indeed because of the huge absorption of the pump radiation within the Nd:YVO_4 AM ($A_a \approx 30.0$ cm^{-1}).

(5) *The laser beam shape influence.* Of a concern are also the features stemming from a particular shape of the laser beam inside the cavity. It is clear that our above analysis has been performed for the effectively rectangular distribution of the beam, while a Gaussian shape of the beam is the more adequate approximation [7,24-27]. However, like in the case of the ESA-effect, there are no principal obstacles to improve our model by

taking the Gaussian distribution of the beam; meanwhile the expected differences with the results reported above shall be of a quantitative character and result in no notable changes in our conclusions.

(6) *The effect of nonlinear polarization azimuth rotation.* As it was noticed above, this effect stemming from the latent anisotropy of dopants in a passive Q-switch and observable in the Nd-lasers on garnet crystals [7,10,24,28], is fully eliminated in the lasers with the ortho-vanadate highly-anisotropic Nd-doped crystals and thus is out of the present study's scope.

References

1. Cai, Z.P., Xu, H.Y., and Stéphan, G., Opt. Commun., 1997, **135**, 295.

2. N.N.Il'ichev, A.V.Kir'yanov, P.P.Pashinin, and S.M.Shpuga, JETP, **78** (1994) 768-777.

3. S.Camacho-Lopez, R.P.M.Green, G.J.Crofts, and M.J.Damzen, J. Mod. Opt., **44** (1997) 209-219.

4. N.N.Il'ichev, A.V.Kir'yanov, and A.A.Malyutin, Sov. J. Quant. Electron., **21** (1991) 844-848.

5. N.N.Ilichev, A.V.Kir'yanov, A.A.Malyutin, P.P.Pashinin, and S.M.Shpuga, Las. Phys., **3**, (1993)182-192.

6. W. Koechner, Solid State Laser Engineering, New York: Springer-Verlag, (1976). Ch. 8.

7. N.N.Il'ichev, A.V.Kir'yanov, E.S.Gulyamova, and P.P.Pashinin, Quant. Electron., **28**, (1998). 17-20

8. A.V.Kir'yanov, V.Aboites, and I.V.Mel'nikov, Appl. Phys. Lett., **78** (2001) 874-876.

9. J.H.Garcia-Lopez, V.Aboites, A.V.Kir'yanov, M.J.Damzen, and A.Minassian, Opt. Commun.,**218** (2003) 155-160.

10. N.N.Il'ichev, A.V.Kir'yanov, and P.P.Pashinin, Quant. Electron., **28** (1998) 147-151.

11. A.Brignon, JOSA B, **13** (1996) 2154-2163.

12. Y.-F.Chen, S.W.Tsai, and S.C.Wang, Opt. Lett., **25** (2000) 1442-1444.

13. A.Agnesi and S.Dell'acqua, Appl. Phys. B, **76** (2003) 351-354.

14. Y.-F.Chen, S.W.Tsai, S.C.Wang, and J.Chen, Appl. Phys. B, **73** (2001) 115-118.

15. Y.-F.Chen, J-L.Lee, H.D.Hsieh, and S.W.Tsai, IEEE J. Quant. Electron., **38** (2002) 312-317.

16. W.deRossi, F.E.Costa, N.D.Viera Jr., N.U.Wetter, S.P.Morato, T.T.Basiev, V.A.Konyushkin, and S.B.Mirov, Appl. Opt., **31** (1992) 2719-2721.

17. D.Y.Tang, S.P.Ng, L.J.Qin, and X.L.Meng, Opt. Lett., **28** (2003) 325-327.

18. J.C.Bermudez G., V.J. Pinto-Robledo, A.V.Kir'yanov, and M.J.Damzen, Opt. Commun., **210**, (2002) 75-82.

19. Z.Xiong, Z.G.Li, N.Moore, W.L.Huang, and G.C.Lim, IEEE J. Quant. Electron., **39** (2003) 979-986.

20. A.Sennaroglu, Appl. Opt., **36** (1997) 9528-9535.

21. J.Song, C.Li, and K.Ueda, Opt. Commun., **177** (2000) 307-316.

22. A.V.Kir'yanov, Yu.O.Barmenkov, M. del Rayo, and V.N.Filippov, Opt. Commun., **213** (2002)151-162.

23. M.A.Jaspan, D.Welford, and J.A.Russel, Appl. Opt., **43** (2004) 2555-2560.

24. N.N.Il'ichev, E.S.Gulyamova, and P.P.Pashinin, Quant. Electron., **27** (1997) 972-977.

25. X.Zhang, S.Zhao, Q.Wang, B.Ozygus, and H.Weber, JOSA B, **17** (2000) 1166-1175.

26. J.K.Jabszynski, J.Kwiatkowski, and W.Zendzian, Opt. Expr., **11** (2003) 552-559.

27. G.Li, S.Zhao, H.Zhao, K.Yang, and S.Ding, Opt. Commun. (2004), available in www.sciencedirect.com.

28. G.Bouwmans, B.Segard, and P.Glorieux, Opt. Commun., **196** (2001) 257-268.

Chapter 4. Diode side-pumped Nd:YVO_4 laser Q-switched with LiF:F_2^- saturable absorber.

4.1 Introduction

The experiment and theoretical modeling of a Passive Q-switching (PQS) of a diode-side-pumped Nd:YVO4 laser using a LiF:F2- crystal as a saturable absorber are presented in this chapter. A grazing-incidence geometry was applied to the cavity, and trains of giant pulses of minimal duration of ~10 ns and peak power of hundreds watts were obtained. The laser efficiency and beam quality in the PQS regime are shown to strongly depend on the cavity arrangement and output coupler reflectivity. In particular, maximum of average output of 18.5 W at high-quality (TEM_{00} mode) PQS operation is obtained at pump power of 38 W at the asymmetrical cavity coupled by a mirror with reflectivity 30%.

4.2 Experiment

A schematic sketch of a side-pumped PQS Nd:YVO_4 / LiF:F_2^- laser is shown in Fig.4.1.

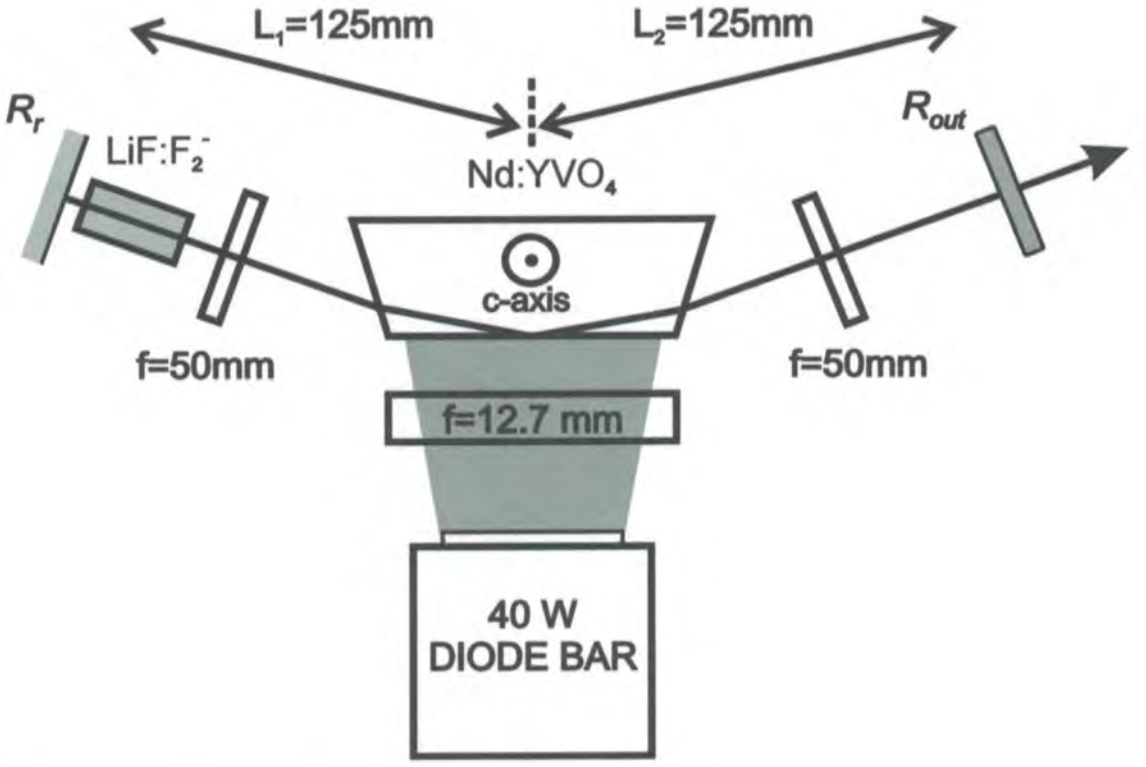

Fig.4.1. Schematic of Nd:YVO_4 laser passively Q-switched with LiF:F_2^- SA.

The experiment was performed with a laser on a c-cut Nd:YVO_4 crystal slab [1] operating at the wavelength 1064 nm and pumped by a semiconductor diode laser bar with the emitting line centered at the wavelength 808 nm. The Nd:YVO_4 slab (2 X 5 X 20 mm) pumped face had an AR coating for the wavelength 808 nm, whereas its front and end faces (slightly tilted at 5° to prevent self-lasing) were AR coated for the wavelength 1064 nm. The crystal was mounted between two aluminum plates and an indium foil ensured good thermal contact. The bottom plate was contacted with a thermoelectric cooler (TEC), controlling the plate temperature via monitoring a thermistor mounted on a copper conduction plate. The TEC bottom was attached to a water-cooled heat sink with thermal grease at the interface. The heat sink was connected to a second chiller unit and the water temperature was fixed at 17° C.

The pumping laser diode bar was conduction-cooled by a water-cooled heat sink dissipater, which temperature was kept at 27°C to obtain the optimum diode-pumping wavelength of 808 nm. The diode was equipped with a face-axis collimator and a cylindrical lens to form a focused strip on the Nd:YVO_4 crystal pumped face with the dimensions of ~ 0.1 X 15 mm. Maximum launched CW power from the pumping laser diode was 38 W.

The laser cavity was designed in a grazing-incidence configuration, where a laser beam experiences a bounce (total internal reflection) at the slab pumped face. The internal grazing-incidence angle was ~ 6 - 8°. The cavity was formed by a pair of plane mirrors:

The rear back mirror had reflectivity R_r = 100% and the output coupling mirror - R_{out} = 30, 50, and 90%. Two cylindrical lenses of 50 mm focal length were placed inside the cavity close to the Nd:YVO_4 crystal to provide maximum coupling of radiation with the pumped volume. The geometrical length of the cavity was varied in the course of experiments from ~ 25 cm (a symmetrical cavity configuration shown in Fig. 4.1) to ~ 50 cm (an asymmetrical cavity configuration shown in Fig.4.5(a)).

The PQS regime in the laser was provided by the presence in the cavity (near the rear mirror, see Fig.4.1) of a LiF:F_2^- crystal. The initial (weak-signal) transmission of the LiF:F_2^- SA at the wavelength 1064 nm was ~ 35% and an estimate for its fully bleached transmission is ~ 85–90%. The length of the LiF:F_2^- element was 4 cm; its front and end faces were not AR coated, but this didn't insert much extra intracavity losses because of the low value of the LiF host refractive index m_s = 1.38. The LiF:F_2^- crystal was mounted on a water-cooled stage, that provided its translation control. Because of the presence of the intra-cavity cylindrical lenses the relative geometric cross-sections of the generation spot-sizes on the LiF:F_2^- SA and Nd:YVO_4 AM were approximately 3:1 and 4:1.

There were no additional elements in the cavity, since the role of a spatial diaphragm was played by the pumped area of AM which effectively selects the transversal modes and the role of a polarizer – by the c-cut Nd:YVO_4 AM itself, being a highly polarizing optical material.

The experimental results obtained at the symmetrical cavity configuration (fig.4.1) are shown in figs.4.2–4.4.

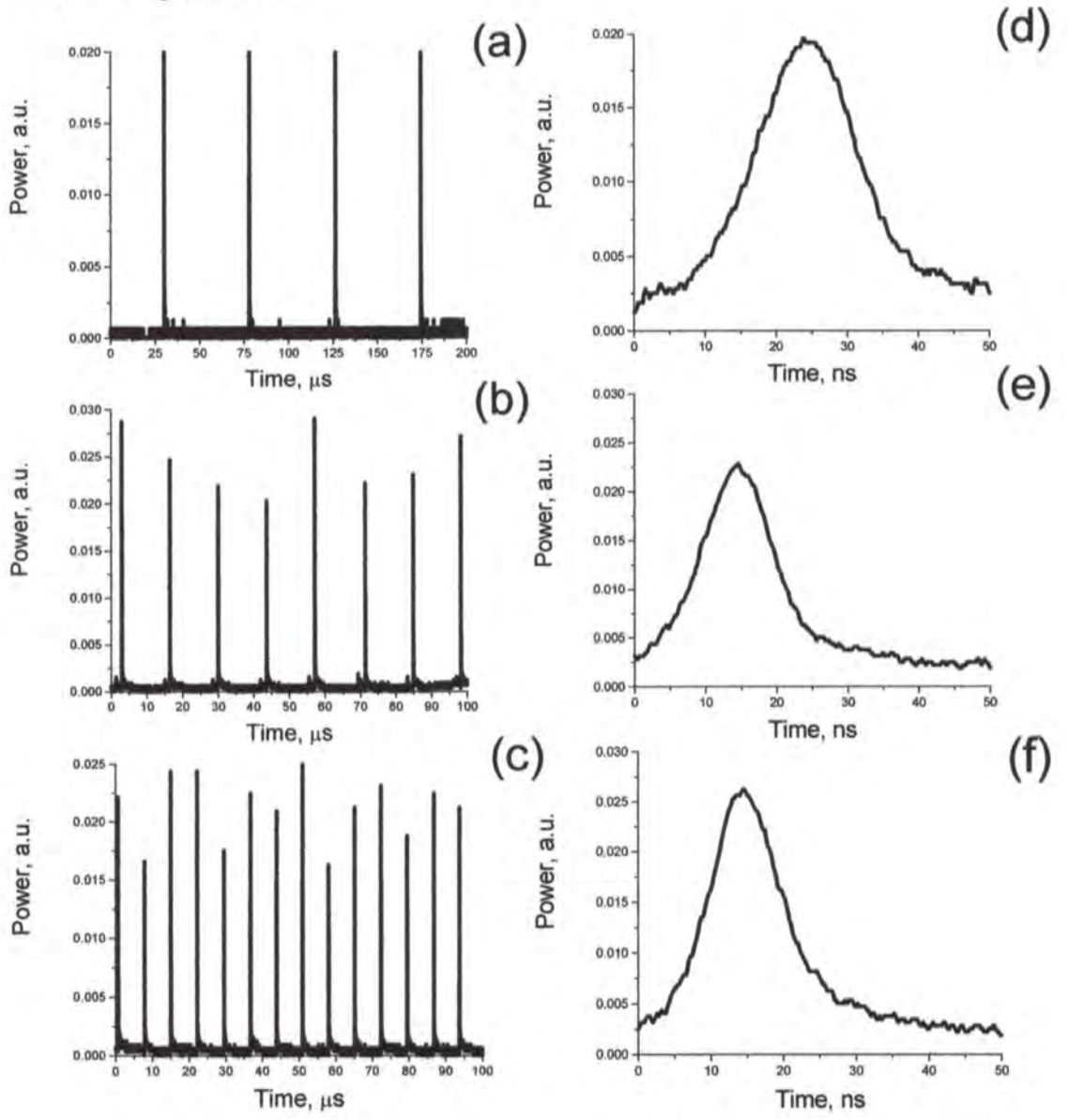

Fig.4.2. (a - c) Trains of GPs and (d – f) portraits of separate pulses obtained at different pump powers (P_p = 14, 26, and 38 W) and R_{out} = 90%. The correspondent average output powers P_{out} = 0.46, 1.21, and 1.92 W.

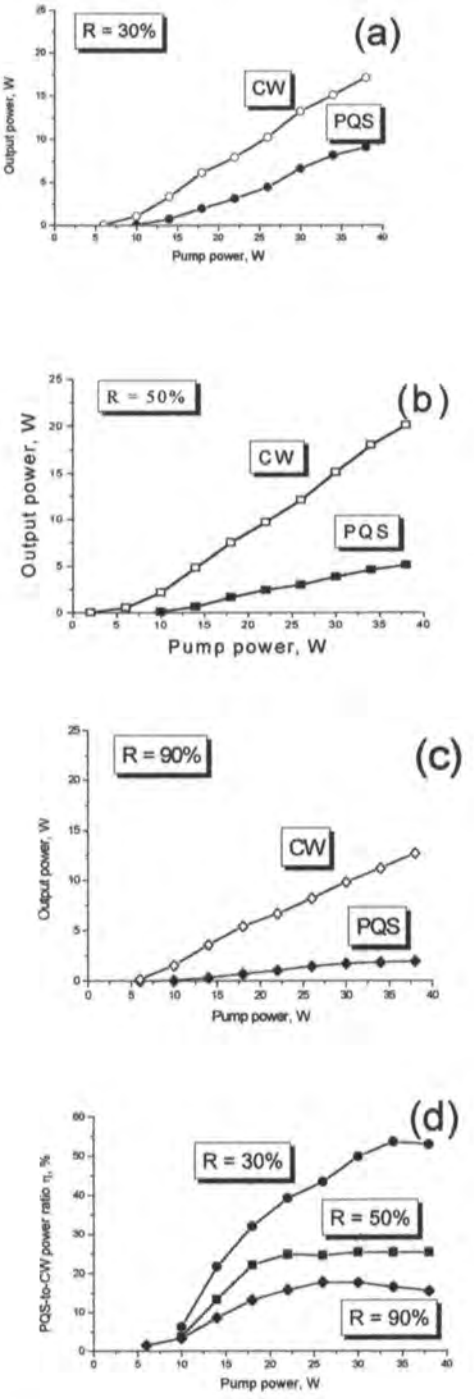

Fig.4.3. (a - c) Experimental dependences of average output power in CW (dashed lines, empty symbols) and PQS (solid lines, filled symbols) regimes versus pump power for R_{out} = 30% (a), 50%(b), and 90%(c). (d) The correspondent dependences of ratios η (output power in PQS regime to that in CW regime) versus pump power.

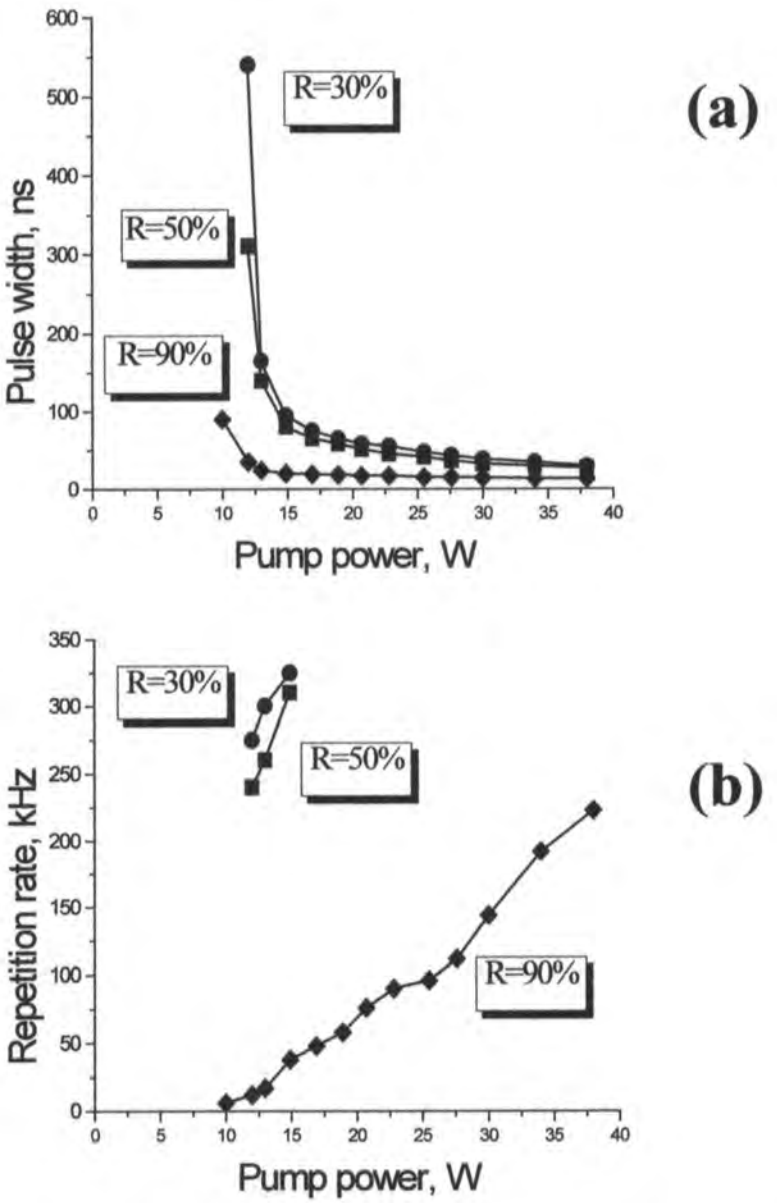

Fig.4.4. Experimental dependences of (a) GP duration and (b) repetition rate versus pump power obtained at different reflection coefficients of output coupler.

Fig.4.2 shows typical GPs generated by the laser at rout = 90% and obtained at different pump powers – P_p = 15 (a), 26 (b), and 34 (c) W, where the left-handed graphs are the snapshots of GP-trains and the right-handed ones – the individual pulses. It is seen from the left-handed graphs that at low pump powers (fig.4.2(a)) GPs in the train are very stable in amplitude and width, whilst at the pump increase (fig.4.2(b) and (c)) pronounceable instabilities in GPs' amplitude appear. As it is normal in PQS lasers, an increase of pump power is accompanied by an increase of repetition rate and decrease of duration (compare the right-handed graphs). The maximum average output power in the PQS regime was P_p = 1.9 W (at P_p = 38 W); peak power of a separate pulse in trains was about 200-300 W and depended weakly on pump power. Note that of a similar behavior was the PQS regime in the laser at a higher reflectivity of the output coupler (R_{out} = 30 and 50%). However, in those cases an increase of pump power is accompanied by more instabilities in the GPs' amplitude and an appearance of pronounceable jitter. The modal structure of the laser output radiation changed with an increase of pump powers: Starting generation with the TEMoo distribution at lower pumps, the laser beam became of the multimode character at higher pumps.

Fig.4.3 (a)-(c) demonstrates the differences in output average power in the PQS regime (filled symbols) obtained for a row of the output mirrors (R_{out} = 30, 50, and 90%); for a comparison, at the same graphs are shown the correspondent dependences of output power in the CW regime (empty symbols) obtained in the absence of the LiF:F_2^- SA in the cavity. Fig.4.3(d) shows the percentage η of the laser output in the PQS regime relatively to that in the CW regime. It is clearly seen that an increase of R_{out} leads to an increase of

efficiency of the PQS mode (up to η = 50% at R_{out} = 30% and $P_p \geq 30$ W); remember, however, that this is accompanied by a serious worsening of the temporal and spectral quality of the output radiation (see above).

Fig.4.4 shows the dependences of GP duration (a) and repetition rate (b) on pump power (curves 1,2, and 3 correspond, respectively, to R_{out} = 90, 50, and 30%). Firstly, one can observe (see fig.4.4(a)) the tendency of a decrease of pulse width at an increase of R_{out} and its weak dependence on pump power if an access of the pump over threshold is more than 1.5. Note also that the minimal GP width is about 10 ns that is attainable at R_{out} = 90%. Secondly, repetition rate of GPs in a train (see fig.21(b)) is averagely proportional to pump power (curve 1); however, certain deviations from the linear law are seen – most probably, because of the mentioned changes in the modal structure of the laser beam occurring at the pump power rise. In addition, one can plot the graphs for repetition rate at R_{out} = 30 and 50% for the pumping range being only a bit above the threshold value (up to 15 W). At higher pump powers, an appearance of jitter between GPs in a train and of additional (lower-power) pulses owing to the multi-mode output structure (see above) makes it impossible to determine repetition rate of GPs. More physical reasoning for the last observations is addressed below.

Finally, fig.4.5 demonstrates the main experimental features of the Nd:YVO_4 / $LiF:F_2^-$ laser optimized both for the maximum average output power and the highest beam-quality in the PQS regime.

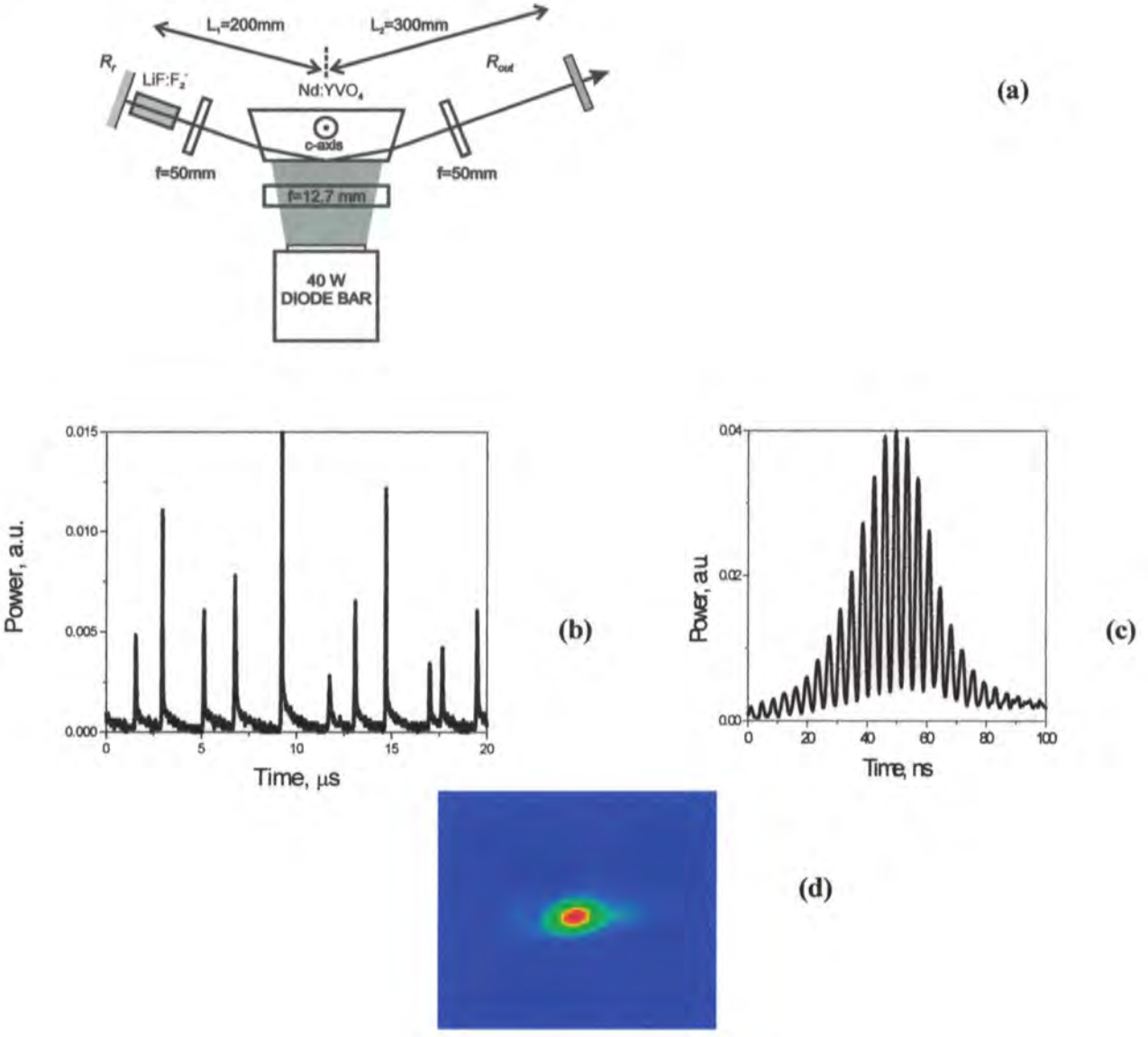

Fig.4.5. (a) Schematic of Nd:YVO_4 / $LiF:F_2^-$ laser optimized for high-beam-quality, high-power operation. (b - c) Typical TEMoo distribution of output laser beam (b); train of GPs (c); single GP demonstrating self-mode-locking effect (d). Pump power – P_p = 38.0 W; average output power – P_{out} = 18.5 W.

A fine alignment of the cavity has allowed us to find its optimal configuration, the asymmetrical design (Fig.4.5(a)), where the coupling mirror R_{out} = 30%. The maximum average output power accessible in this case was $P_{out} \approx$ 18.5 W at P_p = 38 W. The correspondent modal structure of the laser beam is shown in Fig.4.5(d); it is seen that the laser operated in the TEM_{00} mode. However, like in the previous experiments, GPs were seriously modulated in amplitude and a pronounceable jitter is observed between the pulses (fig.4.5(b)). The latter is a certain drawback of the PQS regime as it doesn't allow one to ensure short-term stability of the parameters. Note that once the Nd:YVO_4 / LiF:F_2^- PQS laser is optimized for the TEM_{00} -operation a partial self-mode-locking effect is registered (Fig.4.5(c)), which resembles the phenomenon annotated in Ref.2. In the latter case, each GP is modulated on the mode-beating frequency ($\approx$ 266 MHz) that corresponds to the traveling time of a photon in the cavity. It is interesting to notice that this effect is vanishing when the laser beam is far from the perfect TEM_{00} mode (see, for instance, the right-handed snapshots in fig.4.2).

4.3. Modeling

The dynamics of a PQS Nd:YVO_4 / LiF:F_2^- laser is governed by the rate equations:

$$\frac{dF_a}{dt} = \frac{F_a}{t_R}\left[2\sigma_a N_a l_a - 2\sigma_s l_s n_s - \ln\left(\frac{1}{r_{out}}\right) - \alpha\right] + k\frac{N_a}{\tau_a}, \tag{4.1}$$

$$\frac{dN_a}{dt} = -\gamma\sigma_a N_a F_a c - \frac{N_a}{\tau_a} + R_p\left(N_{tot} - N_a\right), \tag{4.2}$$

$$\frac{dn_s}{dt} = -\sigma_s n_s F_a c K + \frac{n_s^0 - n_s}{\tau_s}, \tag{4.3}$$

where the variables are as follows: F_a, the average photon density inside the cavity; N_a, the population inversion in AM; and n_s, the ground state populations of the F_2^- color centers in the LiF lattice. The parameters entering the equations are: σ_a, the AM lasing cross-section; N_{tot}, the concentration of active (Nd) ions in AM; σ_s, the LiF:F_2^- resonant absorption cross-section caused by F_2^- color centers; l_a and l_s, the lengths of AM and SA, respectively; $K = S_a/S_s$, the ratio of the transverse spot-size of the laser beam in AM to that in SA; r_{out}, the reflection coefficient of the output mirror (useful loss); $\alpha = \alpha_0 + \beta_0$, the overall non-resonant losses (composed of the passive cavity loss α_0 and the loss $\beta_0 = -\ln(T_{fin})l_s$ related to incomplete bleaching of SA at high intensities, where T_{fin} is the full-bleached transmission coefficient of SA); γ, the AM population inversion reduction factor; t_R, the round-trip time of light in the cavity of the optical length L ($t_R = 2L/c$; $L = 1 + l_a m_a + l_s m_s$, where m_a and m_s are the effective refractive indices of the YVO_4 and LiF hosts, respectively, and c is the velocity of light); τ_a and τ_s, the relaxation times of the Nd:YVO_4

AM population inversion and LiF:F_2^- SA excited-state, respectively; k, the factor accounting for the spontaneous radiation in the laser mode; and R_p, the volumetric pump rate.

The two important parameters completing the model are n_s^0, the initial (non-disturbed) ground-state population of F_2^- color centers, and N_a^{in}, the initial (threshold) value of population inversion in the Nd:YVO_4 AM, are defined respectively as follows: $n_s^0 = -\frac{\ln\left(\frac{T_{in}}{T_{fin}}\right)}{\sigma_s l_s}$ (where T_{in} is the initial, or weak-signal, transmission coefficient of SA at the wavelength 1064 nm) and $N_a^{in} = \frac{\alpha + \ln\left(\frac{1}{r}\right) - 2\ln\left(\frac{T_{in}}{T_{fin}}\right)}{2\sigma_a l_a}$ (this formula is obtained at neglecting the last term in Eq.(4.1), which answers to the contribution of spontaneous emission in the laser mode).

Note that Eqs.(4.1-4.3) do not account for the nonlinear absorption anisotropy in a crystalline SA [3,4] and the nonlinear polarization rotation effect in the laser since the first phenomenon is not pronounceable in the case of the LiF:F_2^- crystal [5], contrary to the case of, say, YAG:Cr^{4+} crystal [6], and the second one is almost eliminated in a laser with Nd:YVO_4 AM (this anisotropic crystal dictates a linear state of polarization established in the laser, being fortunately fixed through the whole lasing cycle, contrary to the case of lasers based on the Nd-garnet AM [7,8]).

Finally, the pump volumetric rate R_p in Eq.(4.2) is calculated using the following formula: $R_p = \frac{P_p\left(1-e^{-\Lambda_a l_a}\right)}{S_p l_a h\nu_p \zeta N_{tot}}$, where P_p is the launched diode pump power, $S_p l_a$ is the AM pumped volume, and $\zeta = \lambda_p/\lambda_g$ is the Stokes-loss parameter given by the pump-to-generation wavelength ratio. Note that because of a huge absorption coefficient Λ_a of Nd:YVO_4 at the pump wavelength, the expression in brackets is practically equal to 1 (in other words, the pump power P_p is completely absorbed within the active crystal).

Eqs.(4.1-4.3) are calculated numerically, allowing one to obtain the main characteristics of the PQS Nd:YVO_4 / LiF:F_2^- laser, i.e., the range of pump powers where the PQS regime is supported and the laser basic parameters – average output power; GP energy, duration, and peak power; repetition rate of GPs in a train – and to compare these values with the experimental ones presented above.

4.4 Results and discussion

Since the problem (4.1-4.3) involves many parameters to be varied in principle, we shall further stop on an analysis of a particular case relating to the experimental arrangement shown in fig.4.1. The input parameters are fixed as follows:

Nd:YVO_4 AM: c-cut, $\Lambda_a = 30.0$ cm^{-1}, $N_{tot} = 1.37 \times 10^{20}$ cm^{-3}, $\sigma_a = 2.5 \times 10^{-18}$ cm^2, $\gamma = 1.0$, $\tau_a = 100 \times 10^{-6}$ s, $S_a = 1.5 \times 10^{-3}$ cm^2, $m_a = 2.06$, $l_a = 2.0$ cm; *LiF:F_2^- SA:* (100)-cut, $\sigma_s = 1.2 \times 10^{-17}$ cm^2, $\tau_s = 0.1 \times 10^{-6}$ s, $m_s = 1.37$, $l_s = 4.0$ cm, $T_{in} = 35\%$, $T_{fin} = 85\%$; *laser cavity:* $l = 25$ cm (giving the total optical cavity length $L \approx 34$ cm), $\alpha_0 = 0.1$ (composed of all intra-cavity losses, ~0.01, and Fresnel losses on working surfaces of LiF:F_2^- crystal, ~0.09), $R_r = 100\%$, $R_{out} = 30$, 50, and 90%; *other parameters:* generation wavelength $\lambda_g = 1.06 \times 10^{-4}$ cm (quanta energy $h\nu_g = 1.85 \times 10^{-19}$ J), pump wavelength $\lambda_p = 0.808 \times 10^{-4}$ cm (quanta energy $h\nu_p = 2.45 \times 10^{-19}$ J), $\zeta = 0.76$, $k = 10^{-7}$, $c = 3 \times 10^{10}$ cm, $t_R \approx 2.0 \times 10^{-9}$ s.

The total non-resonant intra-cavity losses are $\alpha = \alpha_0 + \beta_0 l_s = 0.26$ (where $\beta_0 = 0.16$). Therefore, the initial (threshold) value of the population inversion in AM is $N_a^{in} = 2.14 \times 10^{17}$ cm^{-3} and the non-disturbed F_2^- center ground-state population (LiF:F_2^- SA) is $n_s^0 = 1.85 \times 10^{16}$ cm^{-3}, respectively. Also, we take for simplicity that the geometrical cross-sections of the pump and generation waves inside the Nd:YVO_4 AM are the same: $S_p = S_a$.

The modeling results are shown in figs.4.6,4.7. As it is seen from fig.4.6, the theoretical curves P_{out} (P_p) built for R_{out} = 90 (a) and 30% (b) fit quite adequately the correspondent experimental results (in both cases of the PQS and CW operations). Some mismatch between the theoretical and experimental data, seen for the pump values near the threshold, may, most probably, be related to the dynamics of the beam modal structure observed experimentally at the pump increase , which is not covered by the present modeling where an effectively rectangular distribution of the laser beam is implied. figs.4.6(c) and 4.6(d) show the correspondent percentages η of the laser output in the PQS regime relatively to that in the CW regime; it is again seen agreement between the experiment and theory.

Fig.4.7 shows the examples of modeling of the dependences of GP width and repetition rate (fig.4.7(a)) versus pump power (for R_{out} = 90 and 30%), which are the contra-parts for the experimental dependences shown in fig.4.4. One can see at least a qualitative agreement between the experiment and the theory. fig.4.7(b) depicts two other important theoretical dependences characterizing the PQS regime – peak power and energy of a single GP versus pump power. Note that the characteristic peak power of GPs estimated experimentally (about 0.2 kW) is in a good agreement with the numerical calculations (about 0.2 kW).

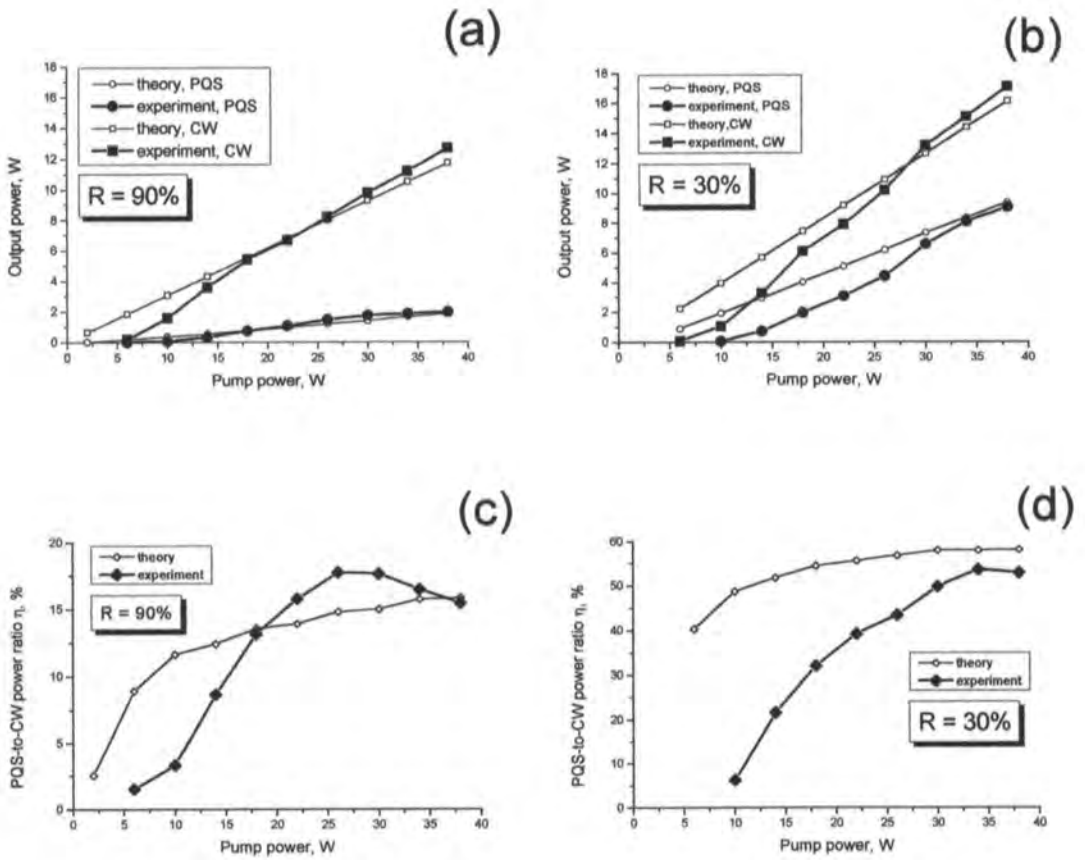

Fig.4.6. (a, b) Theoretical (thin lines, empty symbols) and experimental (thick lines, filled symbols) dependences of average output power in CW and PQS regimes versus pump power for R_{out} = 90% (a) and 30% (b) . (c, d) The correspondent ratios η of output power in PQS regime to that in CW regime versus pump power.

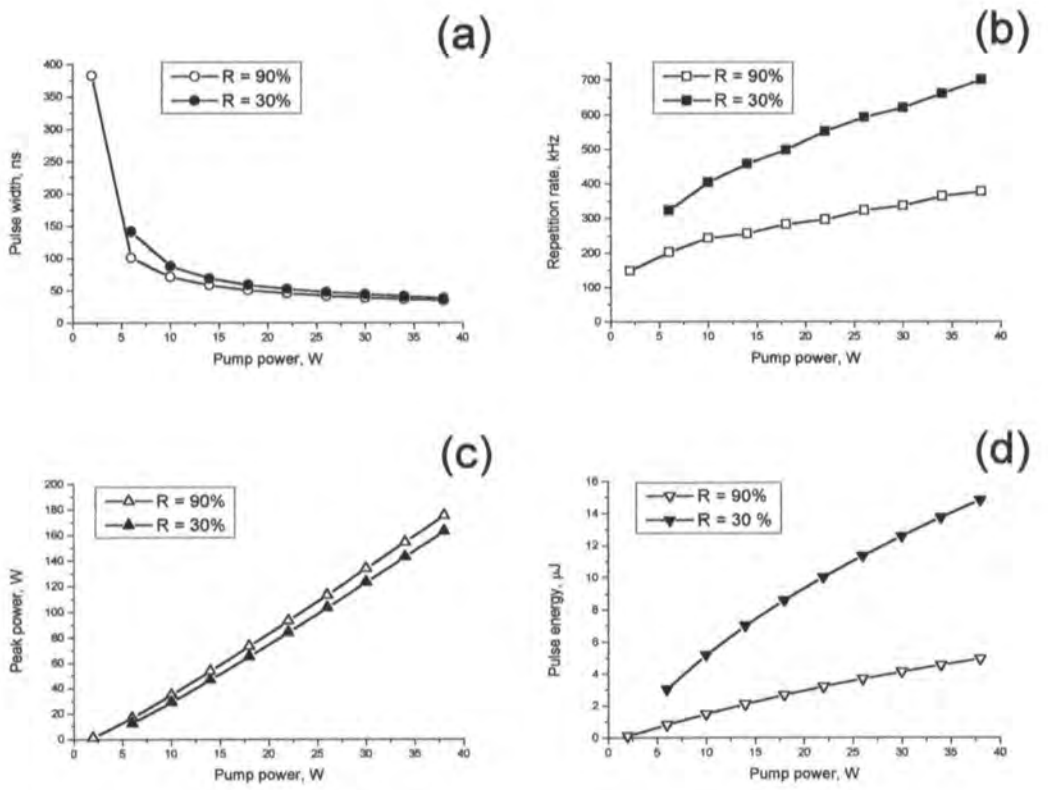

Fig.4.7. (a - d) Theoretical dependences of GP duration (a), repetition rate (b), peak power (c), and energy (d) versus pump power for R_{out} = 90 (empty symbols) and 30% (filled symbols).

Thus, the presented results of modeling allow one a further optimization and principal predicting of main characteristics of a Nd:YVO_4 / LiF:F_2^- PQS laser.

Before to conclude, remind that an unpleasant experimental feature of the PQS regime in the Nd:YVO_4 / LiF:F_2^- laser is instability of GPs' amplitude and jitter, which becomes significant at high pump powers: Beginning from some value of pump power, one cannot even measure repetition rate of GPs in a train (see fig.4.4(b)) since pulses are emitted by the laser chaotically in the time domain. It is not the aim of the present study to treat this feature in detail; however, possible physical sources of this instability are interesting to be annotated here at least.

From one side, one has to re-call to the thermo-induced lensing in AM and SA. This effect has a significant impact on the work of a CW-pumped PQS Nd-laser. At high pump powers, thermo-induced lensing has been shown to be switched on in a Nd:YVO_4 AM [9,10] and LiF:F_2^- SA [11]. Note here that one of possible consequences of this effect, apart from the evident influence on the cavity stability at high pump powers (and transition of the laser from TEM_{00}- to multi-mode- PQS operation), is an appearance of the characteristic frequencies F_{th} (of the kHz-range) in the laser RF-spectrum, corresponding to the times of thermal relaxation $\tau_{th} = \frac{\omega^2 \rho C}{4\kappa}$ in AM and SA (where ρ, C, and κ are, respectively, the density, specific heat, and thermal conductivity of a medium subjected to thermo-loading and ω is the radius of the laser beam in it [12]). The last feature should inevitably disturb the PQS regime and result in the mentioned pronounceable instabilities of the GPs' amplitude and jitter: Each subsequent GP in a train begins to "feel" a preceding one

(through the thermally-induced change in refractive index), starting from a characteristic repetition rate f of GPs' (and thus pump power) when $f \geq F_{th} = 1/\tau_{th}$. Our estimations for the corresponding "thresholds" of the thermally induced instabilities in the laser are $F_{th,SA} \propto 0.1$ kHz (LiF:F_2^-) and $F_{th,AM} \propto 100$ kHz (Nd:YVO_4). A comparison of the experimental features (i.e., the threshold of chaotic emission of GPs by the laser) and the last estimate stemming from the idea of the role of thermo-induced processes in Nd:YVO_4 AM (not in LiF:F_2^- SA) allows one to conclude about its relevance.

On the other hand, certain role in the discussed instabilities (in magnitude of GPs and jitter) may be played by the known effect of irreversible bleaching (decomposition) of F_2^- aggregate color centers in LiF at the two-photon absorption from the excited state at the wavelength 1064 nm [13,14]. This effect, as shown in Refs.15-18, may result in considerable changes in output power and also spectral and polarization characteristics of the PQS regime in a Neodymium laser where a LiF:F_2^- serves as SA. It is clear that in the powerful PQS Nd:YVO_4 / LiF:F_2^- laser treated above, similar effects in the LiF:F_2^- SA have to play a considerable role as well.

Finally, let us notice the nonlinear-dynamics features as a possible source of additional instabilities in the Nd:YVO_4 / LiF:F_2^- system. Such features have been recently reported in [19] for the Nd:YVO_4 / YAG:Cr^{4+} laser which at high pump powers demonstrates all the properties of an autonomous class-B laser, i.e., an appearance of multiple attractors, bifurcations, transition to chaos, etc. So, one can expect that these regimes would be of a similar behavior in the Nd:YVO_4 / LiF:F_2^- laser, too.

References

1. *CASIX, China, product Information (http://www.casix.com)*

2. Chen, Y.-F., Tsai, S.W., Wang, S.C., and Chen, J., 2001, Appl. Phys. B, **73**, 115.

3. Il'ichev, N.N., Kir'yanov, A.V., and Malyutin, A.A., 1991, Sov. J. Quant. Electron., **21**, 844.

4. Camacho-Lopez, S., Green, R.P.M., Crofts, G.J., and Damzen, M.J., 1997, J. Mod. Opt., **44**, 209.

5. Il'ichev, N.N., Kir'yanov, A.V., Malyutin, A.A., et al., 1993, Las. Phys., **3**, 182.

6. Il'ichev, N.N., Kir'yanov, A.V., Pashinin, P.P., and Shpuga, S.M., 1994, JETP, **78**, 768.

7. Il'ichev, N.N., Kir'yanov, A.V., Gulyamova, E.S., and Pashinin, P.P., 1998, Quant. Electron., **28**,17.

8. Il'ichev, N.N., Kir'yanov, A.V., and Pashinin, P.P., 1998, Quant. Electron., **28**, 147.

9. Bermudez J.C.G., Pinto-Robledo V.J., Kir'yanov A.V., and Damzen M.J., 2002, Opt. Commun., **210,** 75.

10. Xiong, Z., Li, Z.G., Moore, N., et al., 2003, IEEE J. Quant. Electron., **39,** 979.

11. Il'ichev, N.N. and Pashinin, P.P., 2000, Laser Phys., **10**, 422.

12. Kir'yanov, A.V., Barmenkov, Yu.O., del Rayo, M., and Filippov, V.N., 2002, Opt. Commun., **213,** 151.

13. Il'ichev, N.N., Kir'yanov, A.V., Malyutin, A.A., et al., 1990, Phys. JETP, **71**, 532.

14. Basiev, T.T., Il'ichev, N.N., Kir'yanov, A.V., et al., 1997, Journ. of Luminisc., **72-74**, 635.

15. Il'ichev, N.N., Kir'yanov, A.V., Malyutin, A.A., et al., 1991, Sov. J. Quant. Electron., **21**, 389.

16. Il'ichev, N.N., Isbasescu, M., Kir'yanov, A.V., et al., 1991, Sov. J. Quant. Electron., **21**, 627.

17. Il'ichev, N.N., Kir'yanov, A.V., Malyutin, A.A., et al., 1994, Quant. Electron., **24**, 570.

18. Il'ichev, N.N., Kir'yanov, A.V., Malyutin, A.A., and Pashinin, P.P., 1994, Quant. Electron., **24**, 577.

19. Tang, D.Y., Ng, S.P., Qin, L.J., and Meng, X.L., 2003, Opt. Lett., **28,** 325.

Chapter 5. Conclusions.

5.1 Comparative analysis of passively Q- switched lasers.

The modeling and comparative analysis of the two CW longitudinally-diode-pumped Nd:YVO_4 lasers Q-switched with the LiF:F_2^- and YAG:Cr^{4+} crystals were developed. The derived system of equations addresses the effect of intensity-dependent transmittance of both the SAs, with taking into consideration of the geometric factor representing the distributions of the orientations of the F_2^- color centers and Cr^{4+} ions relatively to the corresponding crystal hosts. The numerical calculation of the model has been performed, which allows one to get a thorough set of dependences for the main output parameters of the Nd:YVO_4 / YAG:Cr^{4+} and the Nd:YVO_4 / LiF:F_2^- lasers. The analysis of the model's results has shown that the LiF:F_2^- Q-switch has evident advantages over the YAG:Cr^{4+} one in the sense of the assessable range of pump powers, at which the PQS regime is supported in the laser (in the laser with the LiF:F_2^- SA, this range may be more than 20 times wider than in the laser with the YAG:Cr^{4+} SA). As a consequence, higher average output and peak pulse powers may be reached in the Nd:YVO_4 / LiF:F_2^- laser. The physical evidences for these conclusions have been also annotated; the main of them are (i) the significantly higher saturating intensity at the lasing wavelength in the LiF:F_2^- crystal than that in the YAG:Cr^{4+} crystal and (ii) the nonlinear-anisotropy effect in the crystals under the action of the intra-cavity lasing radiation, which, being less-expressed in the LiF:F_2^- SA than in the YAG:Cr^{4+} SA, results in the more expanded (on the pump powers) range where the PQS regime is stable.

5.2 Diode-side-pumped Nd:YVO_4 laser Q-switched with LiF:F_2^- saturable absorber

The first demonstration of the PQS regime in a diode-side-pumped Nd:YVO4 laser with the grazing-incidence geometry of the cavity and a LiF:F2- crystal used as an intra-cavity SA was reported.

At the symmetric plane-plane cavity of the grazing design, we have obtained trains of GPs with minimum duration of ~10 ns and maximum peak power of ~0.5 kW, sequenced at the repetition rate of up to 200 kHz. Maximum average power of the PQS regime, where stable in amplitude and jitter-free GPs are produced, is ~2 W (obtained with an output coupler of R_{out} = 90%). The asymmetric laser cavity at the optimal alignment allows generation of a perfect TEM_{00} mode with maximum average output power of ~18.5 W (at P_p = 38 W). However, GPs in these conditions are chaotically modulated by amplitude and sequenced in the train with pronounceable jitter; a partial self-mode-locking effect has been registered in the latter case.

A theoretical modeling of the PQS Nd:YVO4 / LiF:F2- laser has been also performed and its results have been shown to be in agreement with the experimental data.

Appendix.

Comparative anlysis of CW-pumped Nd:YVO_4 lasers passively Q-switched with LiF:F_2^- and YAG:Cr^{4+} crystals. E. Villafana R and A.V. Kiryanov to be published in Optics Communications.

Diode-side-pumped Nd:YVO_4 laser Q-switched with LiF:F_2^- saturable absorber E. Villafana R., A.V. Kir'yanov A. Minassian, M.J. Damzen to be published in Laser Physics.

A diode pumped high-power Nd:YVO_4 laser passively Q-switched with LiF:F_2^- crystal A.V. Kir'yanov, E. Villafana R., A. Minassian and M. Damzen presented at the EPS-QEOD Europhoton Conference (Lausanne, Switzerland, 2004), paper TuC12.